Monthly Notices
of the
ROYAL ASTRONOMICAL SOCIETY

Mon. Not. R. Astron. Soc. **415,** 1155–1178 (2011) doi:10.1111/j.1365-2966.2011.18691.x

Energetic constraints to chemo-photometric evolution of spiral galaxies

Alberto Buzzoni⋆

INAF – Osservatorio Astronomico di Bologna, Via Ranzani 1, 40127 Bologna, Italy

Accepted 2011 March 10. Received 2011 February 22; in original form 2010 June 29

Downloaded from https://academic.oup.com/mnras/article/415/2/1155/1034920 by INAF –IASF Bologna user on 17 January 2023

ABSTRACT

The problem of chemo-photometric evolution of late-type galaxies is dealt with relying on prime physical arguments of energetic self-consistency between chemical enhancement of galaxy mass, through nuclear processing inside stars, and luminosity evolution of the system. Our analysis makes use of the Buzzoni template galaxy models along the Hubble morphological sequence. The contribution of Type II and Ia SNe is also accounted for in our scenario. Chemical enhancement is assessed in terms of the so-called 'yield metallicity' ($\mathcal{Z}$), that is the metal abundance of processed mass inside stars, as constrained by the galaxy photometric history. For a Salpeter initial mass function (IMF), $\mathcal{Z} \propto t^{0.23}$ being nearly insensitive to the galaxy star formation history. The interstellar medium (ISM) metallicity can be set in terms of $\mathcal{Z}$, and just modulated by the gas fraction and the net fraction of returned stellar mass (f). For the latter, a safe upper limit can be placed, such as $f \lesssim 0.3$ at any age.

The comparison with the observed age–metallicity relation allows us to set a firm upper limit to the Galaxy birthrate, such as $b \lesssim 0.5$, and to the chemical enrichment ratio $\Delta Y/\Delta Z \lesssim 5$. About four out of five stars in the solar vicinity are found to match the expected $\mathcal{Z}$ figure within a factor of 2, a feature that leads us to conclude that star formation in the Galaxy must have proceeded, all the time, in a highly contaminated environment where returned stellar mass is in fact the prevailing component to gas density.

The possible implication of the Milky Way scenario for the more general picture of late-type galaxy evolution is discussed moving from three relevant relationships, as suggested by the observations. Namely (i) the down-sizing mechanism appears to govern star formation in the local Universe; (ii) the 'delayed' star formation among low-mass galaxies, as implied by the inverse $b - M_{\rm gal}$ dependence, naturally leads to a more copious gas fraction when moving from giant to dwarf galaxies; (iii) although lower-mass galaxies tend more likely to take the look of later-type spirals, it is mass, not morphology, that drives galaxy chemical properties. Facing the relatively flat trend of $\mathcal{Z}$ versus galaxy type, the increasingly poorer gas metallicity, as traced by the [O/H] abundance of H II regions along the Sa → Im Hubble sequence, seems to be mainly the result of the softening process, that dilute enriched stellar mass within a larger fraction of residual gas.

The problem of the residual lifetime for spiral galaxies as active star-forming systems has been investigated. If returned mass is left as the main (or unique) gas supplier to the ISM, as implied by the Roberts time-scale, then star formation might continue only at a maximum birthrate $b_{\rm max} \ll f/(1-f) \lesssim 0.45$, for a Salpeter IMF. As a result, only massive ($M_{\rm gal} \gtrsim 10^{11}\,{\rm M}_\odot$) Sa/Sb spirals may have some chance to survive ∼30 per cent or more beyond a Hubble time. Things may be worse, on the contrary, for dwarf systems, that seem currently on the verge of ceasing their star formation activity unless to drastically reduce their apparent birthrate below the $b_{\rm max}$ threshold.

Key words: Galaxy: disc – Galaxy: evolution – galaxies: abundances – galaxies: ISM – galaxies: spiral.

1 INTRODUCTION

A fair estimate of 'galaxy metallicity' has been widely recognized as a basic issue when assessing the distinctive evolutionary properties

⋆E-mail: alberto.buzzoni@oabo.inaf.it

© 2011 The Author
Monthly Notices of the Royal Astronomical Society © 2011 RAS

of late-type galaxies (LTGs), including all disc-dominated systems along the Hubble morphological sequence. However, since both spiral and irregular galaxies consist of a composite stellar population (CSP), the question cannot easily be settled, as it depends on the specific criterion we want to adopt to identify a value of Z (or equivalently of [Fe/H]) ideally representative of the stellar system as a whole.

For example, the youngest stars closely track the chemical composition of gas clouds within a galaxy, and we could therefore refer to their value of Z as the galaxy *actual* metallicity (Z_o). On the other hand, this value may not account for the composition of earlier generations of stars, that however still provide a sizable contribution to galaxy total luminosity. In this regard, one would better like to consider an *effective* metallicity estimate ($Z_{\rm eff}$), by weighting the composing stellar populations with their actual photometric contribution or with the number of star members in each group.

These arguments emerge *'in nuce'* from the seminal analysis of Schmidt (1963), but only Arimoto & Yoshii (1987) extensively dealt with the problem of a fair estimate of the effective metallicity in their LTG models using bolometric luminosity as a weighting factor to account for the relative contribution of the composing stellar populations. With this criterion, by considering a collection of theoretical simple stellar populations (SSPs) with a spread in the values of Z, Buzzoni (1995) showed that the integrated spectral energy distribution (SED) for the aggregate still resembled the spectrum of just one SSP with $\log Z_{\rm eff} = \langle \log Z \rangle$. From her side, Greggio (1997) further refined these arguments, at least in the early-type galaxy framework, emphasizing the difference between average methods such as to lead to $[\langle {\rm Fe/H} \rangle]$ versus $\langle [{\rm Fe/H}] \rangle$. A direct estimate of both Z_o and $Z_{\rm eff}$ is provided by Arimoto & Jablonka (1991, hereafter AJ91) in their LTG models. As expected, the effective metallicity is found to be systematically lower by a 20–30 per cent with respect to the actual one.

Apart from any operational definition, however, one has to remark that the classical approach to galaxy chemical evolution, usually pursued in the literature, mainly proceeds from a dynamical point of view, where chemical composition is tightly related to the kinematical properties of the different stellar populations sharing the galaxy morphological design. Sandage & Fouts (1987) and Koeppen & Arimoto (1990) are striking examples, in this regard, of the empirical and theoretical focus to the problem, respectively. After all, just on these basis Baade (1944) led to his first definition of Populations I and II stars.

However, an even more direct physical argument ties metal abundance to galaxy luminosity evolution. For any gram of metals eventually produced in a galaxy, in fact, one gram of hydrogen has been burnt at some time releasing a fixed amount of energy. As a consequence,*a straightforward relationship must be in place between the actual amount of enriched mass in a galaxy ($M_{\rm YZ}$), in the form of metals plus helium in excess to the primordial abundance, and the past luminosity evolution.* The importance of this constraint, often overlooked even in the recent literature, has been first raised by Wirth (1981) in the context of early-type galaxy evolution, and more explicitly assessed by Pagel (1997). This argument also found a more definite theoretical settlement through the so-called 'Fuel consumption theorem', as proposed by Renzini & Buzzoni (1983, 1986).

Given the range of interesting implications for the study of galaxy evolution, we want here to further investigate the problem of the energetic constraint to chemo-photometric evolution of galaxies, with special attention to the more composite scenario of late-type systems. Our analysis will rely on the template galaxy models developed in Buzzoni (2005, 2002). To better catch the real intention of this paper, we would like to warn the reader that our discussion will proceed as far as possible on analytical bases. This will forcedly require some educated simplifications to the problem (after careful physical assessing, however, of the neglected complications), with the aim of more neatly let to emerge the leading relationships that govern galaxy evolution, and in particular the way these systems (and the Universe as a whole) constrained their chemical composition at the different cosmic epochs.

2 THEORETICAL FUNDAMENTALS

In order to better single out the relevant physical boundaries involved in our problem, we need to consider basically the two main photometric contributions, that constrain overall galaxy luminosity evolution. From one hand, in fact, we can recognize the 'smooth' photometric contribution by stars along their quiescent (namely 'hydrostatic') evolutionary stages, according to a given initial mass function (IMF). On the other hand, one has also to consider the supernova bursting events, that interleave galaxy evolution with short but extremely relevant episodes of mass processing.

Following Clayton (1983), H-burning cycles release 26.731 MeV per ^{4}He particle, while a supplementary amount of 7.274 MeV per ^{12}C nucleus is produced by the 3α He-burning cycle. Overall, the energy budget of the nuclear processes that leads to carbon synthesis in stars reaches a total of

$$W_* = 6.98 \times 10^{18}\ {\rm erg\ g^{-1}}. \quad (1)$$

This specific energy output accounts for the 'quiescent' luminosity emission of a galaxy provided by the non-explosive evolutionary stages of stars along the entire IMF mass range.

A supplementary important source of energy and interstellar medium (ISM) metal enrichment should, however, comprise also the SN explosive events. A quite different elemental pattern characterizes the ISM chemical enrichment in case of SNe Ia, meant to be the main synthesizers of the Fe–Ni elemental group (Chevalier 1976; Nomoto 1980), and SNe II, which stem on the contrary from the core collapse of high-mass stars and mainly supply oxygen and other heavier α-elements (e.g. Matteucci & Greggio 1986; Trimble 1991). Nevertheless, both these events may actually be treated coherently in terms of specific energy release as they take in charge the post-carbon nuclear burning up to iron synthesis (and beyond). Again, following Clayton (1983), whatever the chemical path of nuclear reactions, the atomic binding energy difference implies to release 60.605 MeV per ^{56}Fe nucleus or, equivalently,

$$W_{\rm SN} = 1.03 \times 10^{18}\ {\rm erg\ g^{-1}}. \quad (2)$$

Compared to 'quiescent' nuclear reaction chains, for fixed amount of released energy, explosive nucleosynthesis is therefore roughly a factor of 7 more efficient in the whole Z enrichment of the Universe, selectively involving, however, only the heaviest metal supply (see e.g. Matteucci 2004, for a brief but timely focus on this subject).

2.1 Processed mass by 'quiescent' luminosity evolution

Let us explore first the general case of a system consisting of a CSP, as a result of a roughly continual feeding of fresh stellar generations along the whole photometric history. The nature itself of the problem suggests to consider the total bolometric luminosity of the CSP as a convolution integral of several SSPs continually distributed in time

Downloaded from https://academic.oup.com/mnras/article/415/2/1155/1034920 by INAF –IASF Bologna user on 17 January 2023

according to a given star formation rate (SFR), namely

$$\mathcal{L}_{\rm CSP} = \int \ell_{\rm SSP}(\tau) \otimes {\rm SFR}\, {\rm d}\tau. \quad (3)$$

In Buzzoni (2005) we have shown that SSP bolometric luminosity ($\ell_{\rm SSP}$) smoothly evolves with time according to a simple power law such as $\ell_{\rm SSP}(t) \propto t^{-\alpha}$; for a Salpeter IMF, the power index $\alpha = 0.77$, is virtually independent from the SSP chemical composition.[1] Our template galaxy models considered a disc SFR with a characteristic birthrate, $b = {\rm SFR}_o/\langle {\rm SFR} \rangle$ (see e.g. Miller & Scalo 1979), depending on the morphological type (Kennicutt, Tamblyn & Congdon 1994). The distinctive gas → star conversion efficiency implies for the SFR a power-law time dependence such as ${\rm SFR}(t) \propto t^{-\beta}$, so that $b = (1 - \beta)$ (see Buzzoni 2005, for a full discussion).

Within this framework, the total luminosity of a CSP at time t becomes therefore

$$\mathcal{L}_{\rm CSP}(t) = C \int_0^t \tau^{-\alpha}\, (t - \tau)^{-\beta}\, {\rm d}\tau, \quad (4)$$

with a normalization constant C depending on the total mass of the aggregate. Providing that both $\alpha < 1$ and $\beta < 1$, the integral equation has the Euler Beta function as a straightforward analytical solution. More explicitly, it can also be written as

$$\mathcal{L}_{\rm CSP}(t) = \frac{\Gamma(1-\alpha)\Gamma(1-\beta)}{\Gamma(2-\alpha-\beta)}\, C t^{1-\gamma}, \quad (5)$$

where Γ is the Gamma function and $\gamma = \alpha + \beta$. Compared to a reference epoch t_o, one can simply write

$$\mathcal{L}_{\rm CSP}(t) = \mathcal{L}_{\rm CSP}(t_o) \left(\frac{t}{t_o}\right)^{1-\gamma}. \quad (6)$$

If we integrate the CSP emitting power $\mathcal{L}_{\rm CSP}$ over the entire galaxy life, until time T, this eventually gets the global energy $\mathcal{E}$ released by the nuclear processes to sustain galaxy luminosity until that age.

$$\mathcal{E}(T) = \int_0^T \mathcal{L}_{\rm CSP}(t)\, {\rm d}t = \mathcal{E}_o \left(\frac{T}{t_o}\right)^{2-\gamma}, \quad (7)$$

where $\mathcal{E}_o = [\mathcal{L}_{\rm CSP}(t_o) \times t_o]/(2-\gamma)$.

Clearly, at any time the latter quantity *must* balance the amount of processed mass $M_{\rm YZ}$. With respect to the total CSP stellar mass (that is the total mass ever converted in stars, $M^*(T) = \int_0^T {\rm SFR}(t)\, {\rm d}t$), we have that

$$\left.\frac{M^*_{\rm YZ}}{{\rm M}^*}\right|_T = \frac{W_*^{-1}\mathcal{E}(T)}{\int_0^T {\rm SFR}(t)\, {\rm d}t} = \frac{\mathcal{E}_o}{W_*\, {\rm M}_o} \left(\frac{T}{t_o}\right)^{1-\alpha}, \quad (8)$$

where W_* is the energy-mass conversion factor set by the nuclear burning, according to our previous arguments.[2] Again, we set $M_o = {\rm M}^*(t_o) = \int_0^{to} {\rm SFR}(\tau)\, {\rm d}\tau$ for notation convenience. Interestingly enough, equation (8) shows that the way metals enhance with time in a CSP does *not* depend on the SFR details, being fully modulated on the contrary by the IMF slope, which eventually constrains the CSP luminosity evolution through the power index α. Furthermore, in the same equation, note that a parameter $\mathcal{F} = (\mathcal{E}_o/M_o)/W_*$ can also be regarded as a 'burning efficiency factor', which is a measure of how deeply processed mass has been exploited to produce luminosity.

[1] Our SSP evolution assumes a Salpeter (1955) IMF such as $\mathcal{N}(M) \propto M^{-s}$, with the power index $s = 2.35$ along the accounted stellar mass range from 0.1 to 120 $\rm M_\odot$ (see Buzzoni 2005, 2002 for further details).

[2] Note that W_* directly relates to the total efficiency ϵ of nuclear reactions. According to the Einstein equation, i.e. $\mathcal{E} = \epsilon \Delta M c^2$, we have that $W_* = \mathcal{E}/\Delta M = \epsilon c^2$. This eventually leads to a mass → energy conversion efficiency of $\epsilon = 0.0078$.

Table 1. Reference values at $t = 15$ Gyr for a $10^{11}\, \rm M_\odot$ theoretical CSP with changing star formation properties[a].

β	b	$M_*/\mathcal{L}_{\rm CSP}$ ($\rm M_\odot/L_\odot$)	$\mathcal{L}_{\rm CSP}$[b] ($\rm L_\odot$)	$\mathcal{E}_o/M_o$ $\times 10^{17}$ (erg $\rm g^{-1}$)	$\mathcal{F}$[c]
0.8	0.2	2.42	0.41	8.77	0.126
0.6	0.4	1.82	0.55	8.03	0.115
0.4	0.6	1.44	0.69	7.65	0.110
0.2	0.8	1.19	0.84	7.50	0.108
0.0	1.0	1.02	0.98	7.33	0.105
−0.2	1.2	0.89	1.12	7.21	0.103
−0.4	1.4	0.80	1.25	7.06	0.101
−0.6	1.6	0.72	1.38	6.94	0.099
−0.8	1.8	0.66	1.51	6.84	0.098
−1.0	2.0	0.61	1.64	6.77	0.097

[a] Assuming ${\rm SFR} \propto t^{-\beta}$ and a birthrate $b = 1 - \beta$.
[b] For a $1\, \rm M_\odot$ CSP.
[c] Burning efficiency factor $\mathcal{F} = (\mathcal{E}_o/M_o)\, \rm K^{-1}$.

2.1.1 *Trading mass versus luminosity: the galaxy M/L ratio*

Reference stellar mass (M_o) and the corresponding CSP luminosity [$\mathcal{L}_{\rm CSP}(t_o)$] are, of course, strictly related depending on the SFR details. Relying on the Buzzoni (2005, 2002) theoretical framework, we computed in Table 1 the expected value of the M/L ratio at 15 Gyr for different CSPs (Column 3 in the table) along a range of values of the SFR power index, β (Column 1) and stellar birthrate b (Column 2). These values are representative of the full range of scenarios that characterize disc evolution for the different LTG models. From the values of M/L one can easily derive the expected CSP bolometric luminosity, $\mathcal{L}_{\rm CSP}(t_o)$, as well as the value of $\mathcal{E}_o$ at the reference age (Columns 4 and 5, respectively, of Table 1). Finally, the burning efficiency factor, $\mathcal{F}$, is also computed in Column 6.

As both the total stellar mass and luminosity respond in the same way to the SFR, one has that

$$\left.\frac{M}{\mathcal{L}}\right|_t = \left.\frac{M}{\mathcal{L}}\right|_{t_o} \left(\frac{t}{t_o}\right)^{\alpha}, \quad (9)$$

that is *time evolution of galaxy M/L ratio is a nearly universal law, which only depends on the observing wavelength* and, for bolometric and a Salpeter IMF, scales approximately as $M/L \propto t^{3/4}$.

The SFR enters, on the contrary, by setting the absolute value of M/L, at a given age; for example, when compared to a simple starburst, a smooth star formation will result, on average, in a larger number of young bright stars of high mass at a given age. This means, in general, that M/L decreases with decreasing β. In this regard, a convenient fit to the data of Table 1 provides

$$(M/L)_{15} = \frac{1}{(0.23 + b)} + 0.19, \quad (10)$$

with an rms of ±0.04 on the predicted ratio.

2.2 Supernova processing

The 'quiescent' evolution of galaxy luminosity, as described by previous equations, does not take into account the extra-energy release (and the corresponding extra-metal production) by the SN events. As well known, supernovae display a composite genesis. From one hand, in fact, Type II SNe basically deal with the C/O core collapse of individual stars with conveniently high mass such as to exceed the Chandrasekhar limit near the end of their photometric evolution. On the other hand, a much more composite family of objects (shortly grouped into Type Ia SNe) has to be reconducted

Downloaded from https://academic.oup.com/mnras/article/415/2/1155/1034920 by INAF –IASF Bologna user on 17 January 2023

to binary-star evolution. In this case, the key mechanism deals with the mass transfer between the system members, where a primary (originally more massive) star, in its way to the final white-dwarf (WD) death, acts as a fresh-matter supplier to boost evolution of the secondary member. The latter star will therefore be prompted, at some stage, to feed back the WD with fresh fuel until triggering (under appropriate physical conditions) the fatal detonation on the WD surface.

As is well known, the complexity of this scenario, characterized by a number of unknown or poorly constrained physical parameters (i.e. orbit parameters, total mass of the system, and mass ratio of the members), is the main source of uncertainty even in more explicit and sophisticated models of galaxy chemical evolution (see, in particular, Matteucci & Greggio 1986, for a brilliant assessment of the problem). For this reason, let us try here a simplified approach, just to single out the few leading quantities that constrain our relevant physical output.

2.2.1 *Type II SNe*

Considering first the core-collapse events, originating by the explosion of stars with $M_{\rm up} \gtrsim 8 \pm 1\,{\rm M}_\odot$ (see e.g. Smartt et al. 2009) one has that the expected total number of events per unit SSP total mass can be written as

$$n_{\rm SNII}({\rm SSP}) = \left(\frac{2-{\rm s}}{1-{\rm s}}\right) \frac{[{\rm M}^{1-{\rm s}}]^{120}_{\rm Mup}}{[{\rm M}^{2-{\rm s}}]^{120}_{0.1}}, \qquad (11)$$

where we assume a power-law IMF according to Footnote 1. For a Salpeter case (i.e. $s = 2.35$), and in force of the fact that galaxy SFR does not change much on a time-scale comparable with the lifetime of stars with $M \geq M_{\rm up}$ (namely a few 10^7 yr at most, see e.g. equation 3 in Buzzoni 2002), we have

$$n_{\rm SNII}(t) = 0.126\, M_{\rm up}^{-1.35}\, {\rm SFR}(t) \qquad [{\rm yr}^{-1}({\rm M}_\odot {\rm yr}^{-1})^{-1}]. \qquad (12)$$

For $M_{\rm up} = 8\,{\rm M}_\odot$, this leads to a rate of 7.6×10^{-3} SN II events per year for a SFR $= 1\,{\rm M}_\odot\,{\rm yr}^{-1}$. This figure perfectly matches the empirical rate of $(7.5 \pm 2.5) \times 10^{-3}$ independently obtained by Scannapieco & Bildsten (2005) on the basis of the observed SN rate density within $z \leq 1$ by Dahlen et al. (2004) compared against the cosmic SFR density as measured by Giavalisco et al. (2004).

If $E_{51}^{\rm SNII}$ is the mean released energy associated with each SN event (in units of 10^{51} erg), and recalling the SN-specific energy release as previously discussed, the fraction of enriched stellar mass ($M_{\rm YZ}^{\rm SN}$) along time results in

$$\frac{M_{\rm YZ}^{\rm SNII}}{M^*} = n_{\rm SNII} E_{51}^{II} \frac{10^{51}}{W_{\rm SN}\,{\rm M}_\odot} = 0.061\, M_{\rm up}^{-1.35}\, E_{51}^{\rm SNII}, \qquad (13)$$

where $W_{\rm SN}$ is the energy-mass conversion factor set by the explosive nuclear burning as in equation (2), and $\,{\rm M}_\odot$ is the mass of the Sun. The output of equation (13) is displayed in graphical form in Fig. 1, exploring also different IMF slopes. For $M_{\rm up} = 8 \pm 1\,{\rm M}_\odot$, and $E_{51}^{\rm SNII} = 1.3 \pm 0.3$ (Hashimoto 1995; Thielemann, Nomoto & Hashimoto 1996; Kasen & Plewa 2007) one derives

$$\frac{M_{\rm YZ}^{\rm SNII}}{{\rm M}^*} = 0.0047^{+29}_{-21}. \qquad (14)$$

As for equation (8), note that both $M_{\rm YZ}^{\rm SNII}$ and M^* depend on $\int {\rm SFR}(t){\rm d}t$, so that the $M_{\rm YZ}^{\rm SNII}/M^*$ ratio does depend *neither* on time *nor* on the SFR details, being fully constrained by the IMF slope alone (and by the preferred value of $M_{\rm up}$, as well), as displayed in Fig. 1. As a consequence, the appearance of SN II on the scene of galaxy evolution just enters with a straight offset to metallicity.[3]

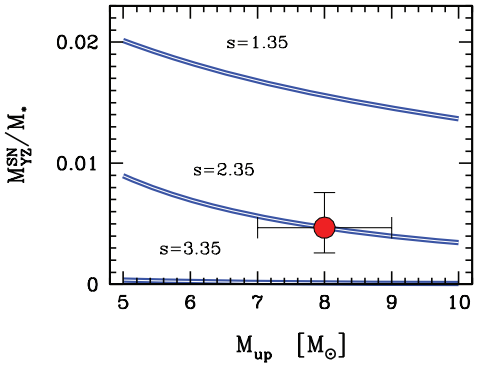

Figure 1. The expected fraction of enriched stellar mass provided by the SN II events according to three different IMF power-law indices (Salpeter case is for $s = 2.35$), and for a different value of the SN triggering mass, $M_{\rm up}$. The consensus case is marked by the big dot on the Salpeter curve. Vertical error bars derive from equation (14).

2.2.2 *Type Ia SNe*

From the theoretical side, Greggio & Renzini (1983) have first argued that the SN Ia population originates from the mix of two stellar components. In fact, the SN detonation may set on both on He-rich WDs (mainly coming from the evolution of relatively low-mass stars, about 2–3 $\,{\rm M}_\odot$), and on the surface of C/O-rich WDs (the final output of more massive stars, about 5–8 $\,{\rm M}_\odot$).[4] This difference, together with the binary nature of the physical mechanism that drives the explosion, makes the total SN Ia rate to depend (at least) on two reference parameters. On the one hand, simple evolutionary arguments on the stellar lifetime set a minimum characteristic 'delay time' ($\Delta_{\rm SNI}$) for the SN burst, which may follow the star formation event (and the first SN II burst) by a few 10^7 yr for CO-rich WDs (Tornambé & Matteucci 1986) up to several 10^8 yr for He-rich WDs (Greggio & Renzini 1983). On the other hand, the broad range of geometric and physical parameters of the binary system may even further displace in time the SN event, blurring the contribution of the two feeding channels into a composite delay-time distribution, namely $\phi_{(\Delta)}(t)$, that we eventually have to deal with.

From the observing side, Mannucci et al. (2005) have firmly demonstrated that SN Ia rate among spiral galaxies tightly relates to the corresponding rate of core-collapsed SNe, the latter meant to closely trace the galaxy SFR. This feature evidently sets important constrains to the $\Delta_{\rm SNI}$ distribution, leading Greggio (2005) to conclude that, in an SSP 'the distribution function of the delay times decreases with time. This means that the majority of SN Ia precursors are relatively short lived'. On this line, Maoz, Sharon & Gal-Yam (2010) argued that over 50–85 per cent of the whole SN Ia population in an SSP are expected to explode within the

[3] Given the special nature of the explosive SN nucleosynthesis, the reported $E_{51}^{\rm SNII}$ value should account for the emitted luminosity, as obtained, for instance, from the time integration of the SN light curve (e.g. Milone & Milone 1988), plus the kinetic energy associated with the SN burst. The latter contribution is actually by far the prevailing one, and it exceeds by about two orders of magnitude the emitted luminosity itself (Woosley & Janka 2005).

[4] In any case, the upper mass of SN I progenitors must be edged by the on-set mass ($M_{\rm up}$) of core-collapsed SNe II.

Downloaded from https://academic.oup.com/mnras/article/415/2/1155/1034920 by INAF –IASF Bologna user on 17 January 2023

first Gyr from the starburst. On the other hand, the residual presence of Type Ia SNe even among quiescent early-type galaxies, that is in lack of any evident star formation activity, calls for a few very delayed events and therefore for a skewed long-term tail of the delay-time distribution (Dallaporta 1973; Mannucci et al. 2005; Panagia, Della Valle & Mannucci 2007; Brandt et al. 2010). Theoretical figures for the SSP case indicate that $\phi_{(\Delta)} \propto t^{-\eta}$, with $\eta \sim 1.2$ (Maoz et al. 2010), or $\sim$2.3, as in the Greggio (2005) or Matteucci & Recchi (2001) models.[5]

Similarly to that already attempted by Scannapieco & Bildsten (2005), we adopt for our discussion the Mannucci et al. (2005) empirical parametrization for the observed SN Ia rate (see equation 2 therein). One can therefore envisage a prevailing term directly related to galaxy SFR and an 'extended' SN fraction (to recall the Scannapieco & Bildsten 2005 original notation), that collects the most delayed events and can therefore be meant to scale at any time with $\int \mathrm{SFR}(t)\mathrm{d}t$, that is with the total stellar mass of a galaxy.

For the first component, the direct SFR dependence is obtained through the core-collapsed SN rate as from equation (12) assuming, with Mannucci et al. (2005), that

$$n_{\mathrm{SNI}} = \begin{matrix} 0.35 n_{\mathrm{SNII}}. \\ \pm\ 8 \end{matrix} \tag{15}$$

By relying then on equation (13), this leads to

$$\frac{M_{\mathrm{YZ}}^{\infty}}{\mathrm{M}^*} = 0.35 \left(\frac{E_{51}^{\mathrm{SNI}}}{E_{51}^{\mathrm{SNII}}} \right) \frac{M_{\mathrm{YZ}}^{\mathrm{II}}}{\mathrm{M}^*}, \tag{16}$$

where the associated energy for a typical SN I event (again, in unit of 10^{51} erg) is of the same order than for SNe II, namely $E_{51}^{\mathrm{SNI}} = 1.5 \pm 0.5$ (Nomoto, Thielemann & Yokoi 1984; Khokhlov, Mueller & Hoeflich 1993; Reinecke, Hillebrandt & Niemeyer 2002; Hillebrandt et al. 2003).

However, the left hand term of equation (16) has to be regarded as a somewhat asymptotic value for the enriched mass fraction as it considers virtually no delay in the SN Ia appearance, being both enriched and total stellar mass perfectly tuned with SFR. If we set SNe Ia to come on the galaxy stage just after the first SN II metal 'glitch', say for $\Delta_{\mathrm{SNI}} \gtrsim 50$ Myr or so, i.e. the reference lifetime for a $5\,\mathrm{M}_{\odot}$ star, then one has to scale previous equation by a factor $(1 - \tau^{\beta-1})$, with $\tau = t/\Delta_{\mathrm{SNI}}$. After this correction, we eventually obtain

$$\frac{M_{\mathrm{YZ}}^{\mathrm{SNI}}}{\mathrm{M}^*} = 0.0019^{+15}_{-13} (1 - \tau^{\beta-1}), \tag{17}$$

where the error bars have been conservatively computed by logarithmic error propagation.

To this contribution one has further to add the long-term 'extended' SN component whose number of events, according to Mannucci et al. (2005), amounts to

$$n_{\mathrm{SNI}}^{\mathrm{ext}\prime} = \begin{matrix} 4.7 \times 10^{-14} \\ \pm\ 9 \end{matrix} \qquad [\mathrm{yr}^{-1}\,\mathrm{M}_{\odot}^{-1}]. \tag{18}$$

This rate is nicely confirmed, within the errors, also by Sullivan et al. (2006).

In case of a star-forming CSP with power-law SFR, the mass-specific event number that occurred up to age T can be written as

$$\left.\frac{N_{\mathrm{SNI}}}{\mathrm{M}^*}\right|_T^{\mathrm{ext}\prime} = n_{\mathrm{SNI}}^{\mathrm{ext}\prime} \left[\frac{\int_{\Delta}^{T} \int_0^t \mathrm{SFR}(\tau)\,\mathrm{d}\tau\,\mathrm{d}t}{\int_0^T \mathrm{SFR}(\tau)\,\mathrm{d}\tau} \right] = \Delta_{\mathrm{SNI}}\, n_{\mathrm{SNI}}^{\mathrm{ext}\prime} \frac{\tau\,(1 - \tau^{\beta-2})}{2 - \beta}. \tag{19}$$

The corresponding amount of processed mass directly derives as

$$\left.\frac{M_{\mathrm{YZ}}^{\mathrm{SNI}}}{\mathrm{M}^*}\right|^{\mathrm{ext}\prime} = \left.\frac{N_{\mathrm{SNI}}}{\mathrm{M}^*}\right|_T^{\mathrm{ext}\prime} E_{51}^{\mathrm{SNI}} \frac{10^{51}}{W\ \mathrm{M}_{\odot}}. \tag{20}$$

By replacing the relevant quantities, we eventually obtain

$$\left.\frac{M_{\mathrm{YZ}}^{\mathrm{SNI}}}{\mathrm{M}^*}\right|^{\mathrm{ext}\prime} = \frac{\Delta_{\mathrm{SNI}}}{2.9 \times 10^{13}} \frac{\tau\,[1 - \tau^{-(1+b)}]}{1 + b}, \tag{21}$$

providing to express the delay time Δ_{SNI} in years.

In conclusion, the relative amount of processed mass related to the whole SN activity in a CSP of SFR power-law index β can be summarized as

$$\frac{M_{\mathrm{YZ}}^{\mathrm{SN}}}{\mathrm{M}^*} = 0.0047 + \begin{cases} 0 & \text{for } \tau < 1 \\ 0.0019\, A(\tau, \Delta_{\mathrm{SNI}}, b) & \text{for } \tau \geq 1, \end{cases} \tag{22}$$

with

$$A(\tau, \Delta_{\mathrm{SNI}}, b) = (1 - \tau^{-b}) + \frac{\Delta_{\mathrm{SNI}}}{5.5 \times 10^{10}} \frac{\tau\,[1 - \tau^{-(1+b)}]}{1 + b}. \tag{23}$$

In Fig. 2, we displayed the relevant output in graphical form, for different ages and values of the SFR power index β. In the plot we also marked the representative values of β for spiral galaxies of different Hubble morphological type, as derived from the Buzzoni (2005) templates.

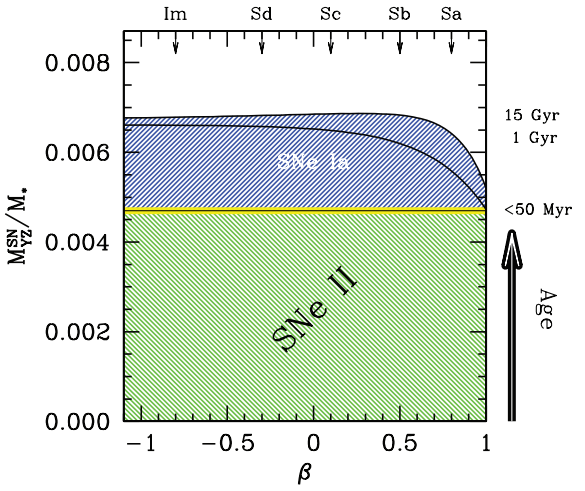

Figure 2. The chemical enrichment from SN contribution according to the different components. Note the prevailing role of core-collapsed objects (i.e. SN II) along the early stages of galaxy evolution ($t \lesssim 50$ Myr, see labels to the right axis). The total SN Ia component adds then a further 0.2 dex to galaxy metallicity, mostly within the first Gyr of life.

2.3 Metals versus helium: the enrichment ratio

With the help of data in Table 1, through equations (6) and (8), it is immediate to derive both disc luminosity (i.e. $\mathcal{L}_{\mathrm{CSP}}$) and the amount of chemically enriched mass (M_{YZ}) along galaxy life.

One may even rely on the expected enrichment ratio $R = \Delta Y/\Delta Z$ to single out the fraction of helium and heavy elements eventually produced. The R parameter can be tuned up either empirically, for

[5] Note that, in all cases, $\eta > \beta$. This assures $\phi_{(\Delta)}$ to fade with time at a quicker rate compared to the reference SFR for our model galaxies. In force of this argument, we can therefore expect the bulk of SN Ia to safely trace the SFR all the time.

Downloaded from https://academic.oup.com/mnras/article/415/2/1155/1034920 by INAF –IASF Bologna user on 17 January 2023

example via the observation of Galactic and extragalactic H II clouds (Lequeux et al. 1979; Serrano & Peimbert 1981; Pagel et al. 1992; Maciel 2001; Peimbert, Peimbert & Luridiana 2002; Casagrande et al. 2007), or theoretically, from stellar evolution theory (Maeder 1992; Marigo, Chiosi & Kudritzki 2003). Some unsettled discrepancies still exist, in this regard, with theory easing in general a more copious production of metals within the stellar population, thus implying a systematically lower value of R compared to the observational evidence. As first pointed out by Mallik & Mallik (1985), this discrepancy might be reconciled from the theoretical side by acting on the IMF upper edge, such as to decrease the expected contribution of the high-mass stellar component. Overall, an admitted range between $R = 3 \pm 1$ is accepted in the literature (e.g. Tosi 1996; Maciel 2001; Fukugita & Kawasaki 2006), and will be considered here.

We could therefore introduce the concept of galaxy *yield* metallicity and helium content defined, respectively, as

$$\begin{cases} \mathcal{Z} = \frac{(M^*_{YZ}+M^{SN}_{YZ})}{M_*}/(1+R) \\ \mathcal{Y} = Y_p + R\,\mathcal{Z}, \end{cases} \tag{24}$$

where $\mathcal{Y} - Y_p$ is the helium abundance, in excess to the primordial content (Y_p).

3 RELEVANT MODEL OUTPUT

The 'yield' abundance of equation (24) can be regarded as the actual mean composition of the bright stars in a CSP at a given epoch. Realistically, $(\mathcal{Z}, \mathcal{Y})$ give a measure of the *maximum* amount of ISM contamination in the evidently extreme case of 'diluting' the entire stellar mass into a vanishing residual fraction of fresh primordial gas. Accordingly, $\mathcal{Z}$ might also be regarded as the maximum value allowed to Z_o, for newly born stars.

Clearly, the real process that leads to ISM chemical enrichment follows from a much more composite scenario, being the result of a continual and subtly entangled interplay between gas and stars inside a galaxy (Tinsley 1980). Actually, this is the central subject of the many important theoretical contributions to the study of chemical evolution of galaxies that have been succeeding along the last few decades (see e.g. Matteucci 2003, for an exhaustive introduction to the subject).

None the less, even facing such a sophisticated reference framework, our simplified approach to chemical enrichment may still be worth of some attention, as the definition of yield metallicity provides us with a straightforward and physically inherent tool to assess the maximum metal abundance that can be reached inside a galaxy at any time. With the study of $(\mathcal{Z}, \mathcal{Y})$ we therefore place a firm constrain to galaxy chemical history in terms of the experienced luminosity evolution. A number of interesting considerations stem from the analysis of the theoretical output of our exercise, mainly dealing with the expected age–metallicity relation (AMR) and with the aged problem of the G-dwarf metallicity distribution.

3.1 The age–metallicity relation

By combining equations (8) and (22) with equation (24) we easily obtain in explicit form the expected AMR for different evolutionary scenarios. With little arithmetic, recalling the $\mathcal{E}_o$ and M_o definitions, the AMR can eventually be set in terms of the integrated properties of the galaxy stellar population:

$$\mathcal{Z}(t) = \frac{0.071}{(1+R)\,(0.23+b)\,(M/L)_{15}}\, t_9^{0.23} + \mathcal{Z}^{SN}, \tag{25}$$

providing to express the reference bolometric M/L ratio[6] at 15 Gyr in solar unit (as from Table 1), and time t_9 in Gyr.[7]

Quite interestingly, note from equation (25) *that time evolution of $\mathcal{Z}$ is almost insensitive to the SFR details*, once considering the M/L versus b inverse dependence, as suggested in equation (10). This is a not so obvious property of the relation, and derives from the nearly constant burning efficiency factor $\mathcal{F}$ of Table 1, that contrasts the amount of released energy from mass processing (namely the $\mathcal{E}_o/M_o$ parameter) with the maximum energy allowed per unit mass (i.e. W_* in equation 8). One sees, from Table 1, that $\mathcal{F}$ varies by less than 20 per cent when moving from a 'bursting' star formation event to a roughly constant or even increasing SFR with time. This makes both M_{YZ} and M^* to scale with b in a similar way. For this reason, the same approximate $\mathcal{Z} \propto t^{1/4}$ dependence has to be expected for a wide range of evolutionary scenarios, including the case of SSP starbursts.

The SN contribution is accounted for, in equation (25), by the term $\mathcal{Z}^{SN} = \frac{M^{SN}_{YZ}}{M_*}/(1+R)$, as from equation (22), where its explicit age dependence, according to the different evolutionary regimes, is constrained by the $A(\tau, \Delta, b)$ function, as in equation (23). As shown in Fig. 2, the effect of SN mass processing quickly reaches a steady contribution to $\mathcal{Z}$ yet within the first Gyr of the galaxy life. For this reason, we can therefore safely set the SN enrichment to

$$\mathcal{Z}^{SN} \simeq 0.0066/(1+R) \tag{26}$$

for any practical application in the framework of our discussion.[8] After accounting for the equation (10) fit, the AMR of equation (25) reduces to

$$\mathcal{Z}(t) = \left[\frac{0.068}{1+0.18\,b}\, t_9^{0.23} + 0.0066\right]\,(1+R)^{-1}. \tag{27}$$

The equation confirms that chemical enrichment of a galaxy disc is a potentially fast process. With $R = 3$, for instance, the solar metallicity is quickly reached within the first few Gyr of the galaxy life, and a current figure about $\mathcal{Z} \simeq 1.5\,Z_\odot$ after one Hubble-time evolution.

The detailed evolution of yield metallicity along the entire Hubble morphological sequence can easily be obtained from the corresponding b values, as summarized in Table 2. A more general display of the $(\mathcal{Z}, \mathcal{Y})$ evolution, for CSPs of different SFR power index β, is displayed in Fig. 3 along the assumed range for the enrichment ratio R. The relevant case for $R = 3$ is also reported in detail in Table 3.

3.1.1 *The AMR in the Galaxy*

A summary of the predicted chemical evolution of the Galaxy from some of the most recognized models in the recent literature is proposed in Fig. 4. In particular, the models by Matteucci & François

[6] Again, the ratio refers to the *stellar* mass, that is the total mass ever converted to stars.

[7] A less direct, but still analytically manageable, form for [Fe/H] versus t could also be obtained, in case, by recalling the basic definition: $[Fe/H] = \log \mathcal{Z} - \log[0.77 - \mathcal{Z}(1+R)] + 1.54$, where we assumed $(Z_\odot, Y_\odot) = (0.02, 0.28)$ for the Sun, and a primordial Helium abundance $Y_p = 0.23$.

[8] To a closer analysis of Fig. 2, our approximation tends to slightly overestimate the right $\mathcal{Z}^{SN}$ figure for more 'bursting' SFRs, as in the case of Sa galaxies. This has no larger impact, however, on our conclusions, as even a fully crude lower estimate such as $\mathcal{Z}^{SN} \simeq 0.0047/(1+R)$ would lead current [Fe/H] predictions for these galaxies to change by much less than 0.03 dex. See Section 4 for an appropriate context to assess this issue.

Downloaded from https://academic.oup.com/mnras/article/415/2/1155/1034920 by INAF –IASF Bologna user on 17 January 2023

Table 2. Photometric properties, reference M/L ratio and yield metallicity at $t = 15$ Gyr for galaxies of different morphological type.[a]

Hubble	Disc component							Whole galaxy[b]
type	β	M_*/L	(Bol − V)	($U - V$)	($B - V$)	($V - K$)	$\mathcal{Z}$	M/L
Sa	0.8	2.42	−0.78	0.60	0.63	2.70	0.033	4.48
Sb	0.5	1.62	−0.78	0.44	0.56	2.59	0.030	3.06
Sc	0.1	1.10	−0.79	0.34	0.51	2.51	0.028	1.86
Sd	−0.3	0.84	−0.80	0.28	0.48	2.46	0.027	1.05
Im	−0.8	0.66	−0.81	0.24	0.46	2.42	0.026	0.66

[a]From Buzzoni (2005) template galaxy models.
[b]Including the spheroid component (i.e. bulge + halo).

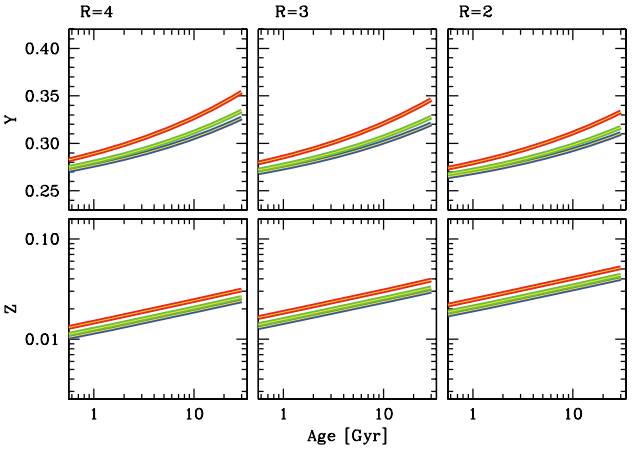

Figure 3. Yield chemical abundance for the CSP set of Table 3. Theoretical output is from equation (24), assuming a range for the enrichment ratio $R = \Delta Y/\Delta Z = 3 \pm 1$, according to the label in each panel. Note the nearly insensitive response of both $\mathcal{Y}$ and $\mathcal{Z}$ to the SFR details.

Table 3. Yield chemical abundance ($\mathcal{Z}$, $\mathcal{Y}$) for CSPs with different SFR and enrichment ratio $R = (\Delta Y/\Delta Z) = 3$.[a]

$R = 3$	Flat or decreasing SFR with time				
	β				
t_9 (Gyr)	0.8 ($\mathcal{Z}$, $\mathcal{Y}$)	0.6 ($\mathcal{Z}$, $\mathcal{Y}$)	0.4 ($\mathcal{Z}$, $\mathcal{Y}$)	0.2 ($\mathcal{Z}$, $\mathcal{Y}$)	0.0 ($\mathcal{Z}$, $\mathcal{Y}$)
1	0.019 0.286	0.017 0.281	0.016 0.279	0.016 0.278	0.016 0.277
1.5	0.020 0.290	0.019 0.286	0.018 0.283	0.018 0.282	0.017 0.281
2	0.021 0.294	0.020 0.289	0.019 0.287	0.019 0.286	0.018 0.285
3	0.023 0.300	0.022 0.295	0.021 0.292	0.020 0.291	0.020 0.289
4	0.025 0.305	0.023 0.299	0.022 0.296	0.022 0.295	0.021 0.293
5	0.026 0.308	0.024 0.302	0.023 0.299	0.023 0.298	0.022 0.296
6	0.027 0.311	0.025 0.305	0.024 0.302	0.023 0.300	0.023 0.299
8	0.029 0.317	0.027 0.310	0.025 0.306	0.025 0.305	0.024 0.303
10	0.030 0.321	0.028 0.314	0.027 0.310	0.026 0.309	0.026 0.307
12.5	0.032 0.326	0.029 0.318	0.028 0.314	0.028 0.312	0.027 0.311
15	0.033 0.330	0.031 0.322	0.029 0.317	0.029 0.316	0.028 0.314
$R = 3$	Increasing SFR with time				
	β				
t_9 (Gyr)	−0.2 ($\mathcal{Z}$, $\mathcal{Y}$)	−0.4 ($\mathcal{Z}$, $\mathcal{Y}$)	−0.6 ($\mathcal{Z}$, $\mathcal{Y}$)	−0.8 ($\mathcal{Z}$, $\mathcal{Y}$)	−1.0 ($\mathcal{Z}$, $\mathcal{Y}$)
1	0.016 0.276	0.015 0.276	0.015 0.275	0.015 0.274	0.015 0.274
1.5	0.017 0.281	0.017 0.280	0.016 0.279	0.016 0.278	0.016 0.278
2	0.018 0.284	0.018 0.283	0.017 0.282	0.017 0.281	0.017 0.281
3	0.020 0.288	0.019 0.287	0.019 0.286	0.019 0.286	0.018 0.285
4	0.021 0.292	0.020 0.291	0.020 0.290	0.020 0.289	0.020 0.289
5	0.022 0.295	0.021 0.294	0.021 0.293	0.021 0.292	0.021 0.291
6	0.023 0.298	0.022 0.296	0.022 0.295	0.022 0.295	0.021 0.294
8	0.024 0.302	0.024 0.301	0.023 0.300	0.023 0.299	0.023 0.298
10	0.025 0.306	0.025 0.304	0.024 0.303	0.024 0.302	0.024 0.301
12.5	0.026 0.309	0.026 0.308	0.026 0.307	0.025 0.306	0.025 0.305
15	0.028 0.313	0.027 0.311	0.027 0.310	0.026 0.309	0.026 0.308

[a]The values of ($\mathcal{Z}'$, $\mathcal{Y}'$) for any other enrichment ratio R' can be derived from the $R = 3$ case, as $\mathcal{Z}' = [4/(1 + R')]\,\mathcal{Z}$ and $\mathcal{Y}' = \mathcal{Y} + [(R' - 3)/(R' + 1)]\mathcal{Z}$.

(1989), Wyse & Silk (1989), Carigi (1994), Pardi & Ferrini (1994), Prantzos & Aubert (1995), Timmes, Woosley & Weaver (1995), Giovagnoli & Tosi (1995), Pilyugin & Edmunds (1996), Mihara & Takahara (1996), as well as by Chiappini, Matteucci & Gratton (1997), Portinari, Chiosi & Bressan (1998), Boissier & Prantzos (1999), and Alibés, Labay & Canal (2001) are considered, along with our $\mathcal{Z}$ law for $b = 0.5 \pm 0.5$, from equation (27).

The whole set of theoretical AMRs is compared in the figure with the empirical AMR in the solar neighbourhood, as obtained by different stellar samples, probing the young O-B stars and the unevolved F-G subgiant population. In particular, six important contributions still provide the reference framework for this analysis, namely the work by Twarog (1980), Carlberg et al. (1985), Meusinger, Stecklum & Reimann (1991), Edvardsson et al. (1993), Rocha-Pinto et al. (2000) and the exhaustive Geneva–Kopenhagen catalogue of stars in the solar neighbourhood (Nordström et al. 2004), recently revised by Holmberg, Nordström & Andersen (2007).

Just a glance at Fig. 4 makes clear the wide spread of theoretical predictions that span nearly a factor of 3 (namely 0.3–0.5 dex in [Fe/H] range) in the expected Galaxy metallicity at a given epoch. For example, newly born stars at $t = 10$ Gyr yet exceed the solar value in the Matteucci & François (1989) model, being as rich as [Fe/H] = +0.11; this is roughly twice the value of the Portinari et al. (1998) model, which predicts on the contrary [Fe/H] = −0.13. Instead of any further speculative attempt to elect the 'right' solution among the many envisaged scenarios (see, however, Romano et al. 2005, for an interesting discussion on this issue), we could rather look at the different theoretical outputs of Fig. 4 as a plain evidence of the inherent uncertainty of any 'deterministic' approach to Galaxy chemical evolution.

It may be useful, however, to try a comparison between models and observations in terms of the same fitting parameters, by approximating the different AMRs with a general power-law evolution such as $Z \propto t^{\zeta}$ or, equivalently, $[\mathrm{Fe/H}] = \zeta \log t_9 + \omega$.[9] In this notation, ζ is the slope of the [Fe/H] versus $\log t$ relationship, as

[9] Of course, this approximation holds as far as the SN term could be neglected, that is for $\mathcal{Z}(t) \gg \mathcal{Z}^{\mathrm{SN}}$.

Downloaded from https://academic.oup.com/mnras/article/415/2/1155/1034920 by INAF –IASF Bologna user on 17 January 2023

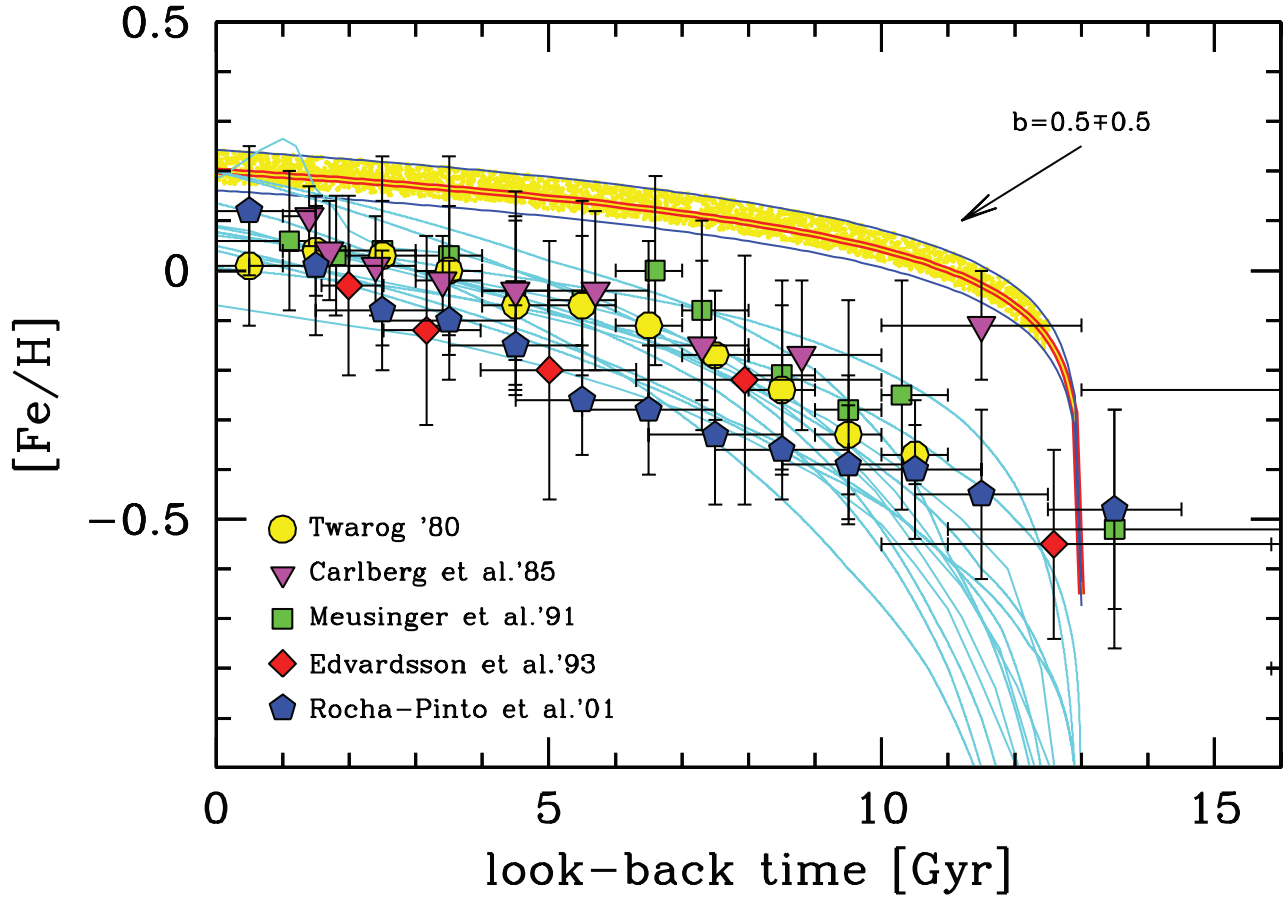

Figure 4. The solar-neighbourhood AMR, according to different observing surveys, as labelled in the plot. In particular, the work of Twarog (1980) (dots), Carlberg et al. (1985) (triangles), Meusinger et al. (1991) (squares), Edvardsson et al. (1993) (diamonds) and Rocha-Pinto et al. (2000) (pentagons) have been considered. Observations are compared with model predictions from several theoretical codes (the shelf of thin curves; see Fig. 5 for a detailed source list). The expected evolution of yield metallicity, according to equation (27), is also displayed, assuming [Fe/H] $= \log \mathcal{Z}/\mathrm{Z}_{\odot}$, and a birthrate $b = 0.5 \pm 0.5$, as labelled on the curve. A current age of 13 Gyr is adopted for the Milky Way. See text for a full discussion.

derived from the fit, while $[\mathrm{Fe/H}]_{10} = \zeta + \omega$ provides the nominal metal abundance of newly born stars at $t = 10$ Gyr. Table 4 and Fig. 5 summarize the results of our fit for the whole set of models analysed, comparing with the corresponding parameters from equation (27) for $R = 3$ and $b = 0.5 \pm 0.5$.

As a striking feature, the plot clearly shows the stronger chemical evolution generally implied by the theoretical codes. The latter predict, in fact, a steeper slope for the [Fe/H] versus $\log t$ relation, exceeding the observed $[\mathrm{Fe/H}]_{10}$ metallicity and predicting a larger value of ζ. To some extent, this untuned behaviour adds further arguments to the delicate role of the gas-infall mechanisms, so extensively invoked by the modern theory. Actually, while sustaining star formation, any external gas supply may even ease metal enhancement, rather than moderate it by diluting processed mass into a larger amount of fresh gas (Larson 1976; Firmani & Tutukov 1992).

3.1.2 *Constraints to the Galaxy SFR*

For its physical definition, yield metallicity provides an upper envelope to the observed AMR, throughout (see, again, Fig. 5). In this regard, it may be useful to further explore this concept, in order to better clarify the link between implied $\mathcal{Z}$ evolution and the observed galaxy AMR.

If we assume that a net fraction $f(t)$ of the stellar mass is returned to the ISM within time t[10], by polluting the residual component of fresh primordial gas (M_{gas}), then the resulting ISM (or, shortly, the 'gas') metallicity, Z_{gas}, must be

$$Z_{\mathrm{gas}}(t) = \frac{f M_{\mathrm{YZ}} (1+R)^{-1}}{M_{\mathrm{gas}} + f M_*} = \frac{f \mathcal{Z}}{(M_{\mathrm{tot}}/M_*) + (f-1)}. \qquad (28)$$

This quantity can be regarded as the representative metallicity of newly born stars. If $\mathcal{S} = M_*/M_{\mathrm{tot}}$ is the mass fraction of 'processed' mass and, accordingly, $\mathcal{G} = 1 - \mathcal{S}$ the fresh (i.e. 'unprocessed') gas fraction then, with little arithmetic, (equation 28) reduces to

$$\left(\frac{Z_{\mathrm{gas}}}{\mathcal{Z}}\right) = \left[\frac{\mathcal{G}}{f(1-\mathcal{G})} + 1\right]^{-1} = \left[\frac{1-\mathcal{S}}{f\mathcal{S}} + 1\right]^{-1}. \qquad (29)$$

As expected, equation (29) shows that, when fresh gas vanishes (i.e. $\mathcal{G} \to 0$), then Z_{gas} tends to $\mathcal{Z}$.

According to equation (28), the total (i.e. fresh + processed) gas fraction can eventually be written as

$$\mathcal{G}_{\mathrm{tot}} = \mathcal{G} + f\,\mathcal{S} = \mathcal{G}\,(1-f) + f. \qquad (30)$$

Whatever the specific model assumptions about the mass recycling

[10] Note that fraction $f(t)$ has to be intended as the *net* balance of the global amount of processed mass returned to the ISM minus the fraction of enriched mass engaged again in later star formation processes.

Downloaded from https://academic.oup.com/mnras/article/415/2/1155/1034920 by INAF –IASF Bologna user on 17 January 2023

Table 4. Fitting parameters for Galaxy theoretical and empirical AMR.[a]

Yield metallicity		
Source	ζ	$[Fe/H]_{10}$
This work[b]	**0.23**	$\mathbf{+0.17 \pm 0.04}$
Models		
Source	ζ	$[Fe/H]_{10}$
Matteucci & François (1989)	0.84	+0.11
Wyse & Silk (1989) ($n = 1$)	0.79	−0.07
” ($n = 2$)	0.49	−0.04
Carigi (1994)	1.14	+0.08
Pardi & Ferrini (1994)	1.04	+0.00
Prantzos & Aubert (1995)	0.76	+0.00
Timmes et al. (1995)	0.42	+0.02
Giovagnoli & Tosi (1995)	1.06	+0.09
Pilyugin & Edmunds (1996)	0.81	−0.06
Mihara & Takahara (1996)	1.28	−0.00
Chiappini et al. (1997)	0.71	−0.00
Portinari et al. (1998)	0.73	−0.13
Boissier & Prantzos (1999)	0.82	+0.02
Alibés et al. (2001)	0.73	−0.03
Observations		
Milky Way 13 Gyr old		
	ζ	$[Fe/H]_{10}$
Twarog (1980)	0.63 ± 0.04	-0.01 ± 0.03
Carlberg et al. (1985)	0.56 ± 0.08	$+0.02 \pm 0.07$
Meusinger et al. (1991)	0.54 ± 0.06	$+0.02 \pm 0.05$
Edvardsson et al. (1993)	0.62 ± 0.12	-0.10 ± 0.11
Rocha-Pinto et al. (2000)	0.88 ± 0.04	-0.05 ± 0.04
Holmberg et al. (2007)	0.30 ± 0.01	-0.12 ± 0.01
Mean of all surveys	$\mathbf{0.59 \pm 0.08}$	$\mathbf{-0.04 \pm 0.03}$

[a]Assuming $[Fe/H] = \zeta \log t_9 + \omega$, with t_9 in Gyr. By definition, $[Fe/H]_{10} = \zeta + \omega$ is the expected metallicity at $t = 10$ Gyr.
[b]From equation (25), for $R = 3$. $[Fe/H]_{10}$ range limits from varying galaxy birthrate $b = 0.5 \pm 0.5$.

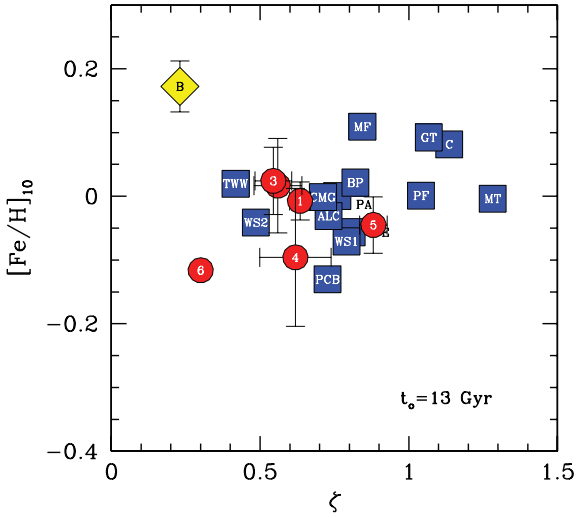

Figure 5. Representative parameters for the observed (dots) and predicted (squares) AMR for the solar neighbourhood. The theoretical works by Matteucci & François (1989) (labelled as ‘MF’ on the plot), Wyse & Silk (1989) (WS1 and WS2, respectively, for a Schmidt law with $n = 1$ and 2), Carigi (1994) (C), Pardi & Ferrini (1994) (PF), Prantzos & Aubert (1995) (PA), Timmes et al. (1995) (TWW), Giovagnoli & Tosi (1995) (GT), Pilyugin & Edmunds (1996) (PE), Mihara & Takahara (1996) (MT), Chiappini et al. (1997) (CMG), Portinari et al. (1998) (PCB), Boissier & Prantzos (1999) (BP) and Alibés et al. (2001) (ALC) have been accounted for, including the expected output from the $\mathcal{Z}$ law of equation (27) (square marker labelled as ‘B’). The Milky Way is assumed to be 13 Gyr old for every model. The theoretical data set is also compared with the observations, according to the surveys of Twarog (1980) (dot number ‘1’), Carlberg et al. (1985) (‘2’), Meusinger et al. (1991) (‘3’), Edvardsson et al. (1993) (‘4’), Rocha-Pinto et al. (2000) (‘5’) and Holmberg et al. (2007) (‘6’). An AMR in the form $[Fe/H] = \zeta \log t_9 + \omega$ is assumed throughout. The displayed quantities are therefore the slope coefficient ζ, versus the expected metallicity at $t = 10$ Gyr, namely $[Fe/H]_{10} = \zeta + \omega$. Note that models tend, on average, to predict a sharper chemical evolution with respect to the observations. This leads, in most cases, to a steeper slope ζ and a slightly higher value for $[Fe/H]_{10}$. See the text for a discussion of the implied evolutionary scenario.

mechanisms, it is clear from the equation that f ends up by driving $\mathcal{G}_{\rm tot}$ when the fresh-gas reservoir is going to be exhausted. This happens, of course, at the very late stages of galaxy evolution. Relying on this definition, equation (29) can also be conveniently arranged in an alternative form such as

$$\left(\frac{Z_{\rm gas}}{\mathcal{Z}}\right) = \left(\frac{f}{1-f}\right)\left(\frac{1-\mathcal{G}_{\rm tot}}{\mathcal{G}_{\rm tot}}\right). \tag{31}$$

As, by definition, $f \leq 1$ a further interesting property of equation (29) is that $(Z_{\rm gas}/\mathcal{Z}) \leq \mathcal{S}$. We can take advantage of this simple constraint to set two important boundary conditions to galaxy SFR. First of all, as $\mathcal{S} \propto t^{1-\beta}$, then it must be

$$\log Z_{\rm gas} - \log \mathcal{Z} \geq (1-\beta)\,\log t + \text{const}. \tag{32}$$

The left hand side of the relation (or its equivalent form in terms of [Fe/H]) simply contrasts the observed AMR in the solar neighbourhood with the expected ‘yield’ metallicity evolution of equation (25). The corresponding analytical functions, for the Milky Way case, can be found in Table 4. In particular, by comparing the relevant slopes, ζ, of the [Fe/H] versus $\log t$ relations one eventually concludes that $\langle \zeta^{\rm AMR} - \zeta^{\rm yield} \rangle \geq (1-\beta)$, which implies, for a current age of 13 Gyr, that

$$b = (1-\beta) \lesssim 0.4 \pm 0.1. \tag{33}$$

The latter constraint simply derives from the fact that, evidently, $(Z_{\rm gas}/\mathcal{Z}) \leq (1-\mathcal{G})$, as well. Therefore, at any epoch, the mass fraction of fresh gas in the galaxy could *at most* be

$$\mathcal{G} \leq 1 - \left(\frac{Z_{\rm gas}}{\mathcal{Z}}\right). \tag{34}$$

Again, by relying on the fitting functions of Table 4, for a 13 Gyr old Milky Way one sees that $\log(Z_{\rm gas}/\mathcal{Z}) \simeq [Fe/H]_{\rm AMR} - [Fe/H]_{\rm yield} = -0.17 \pm 0.05 + \log[(1+R)/4]$, so that the current mass fraction of primordial gas in the Galaxy ($\mathcal{G}_o$) must locate within the range

$$0 \leq \mathcal{G}_o \leq \begin{matrix} 0.17\,(4.9 - R). \\ \pm\ 8 \end{matrix} \tag{35}$$

By the way, this also implies that $R \lesssim 5$, thus setting a useful constraint to the Galaxy enrichment ratio too.

Overall, once compared with the representative SFR properties of the other spiral galaxies along the Hubble morphological sequence (Roberts & Haynes 1994), these figures are consistent with an intermediate Sb type for the Milky Way (e.g. van der Kruit 1986). In particular, according to Buzzoni (2005), the allowed range for the SFR leads to an integrated disc colour about $(B-V) \sim 0.60 \pm 0.05$, in agreement with the empirical evidence (Flynn et al. 2006; Melchior, Combes & Gould 2007).

Downloaded from https://academic.oup.com/mnras/article/415/2/1155/1034920 by INAF –IASF Bologna user on 17 January 2023

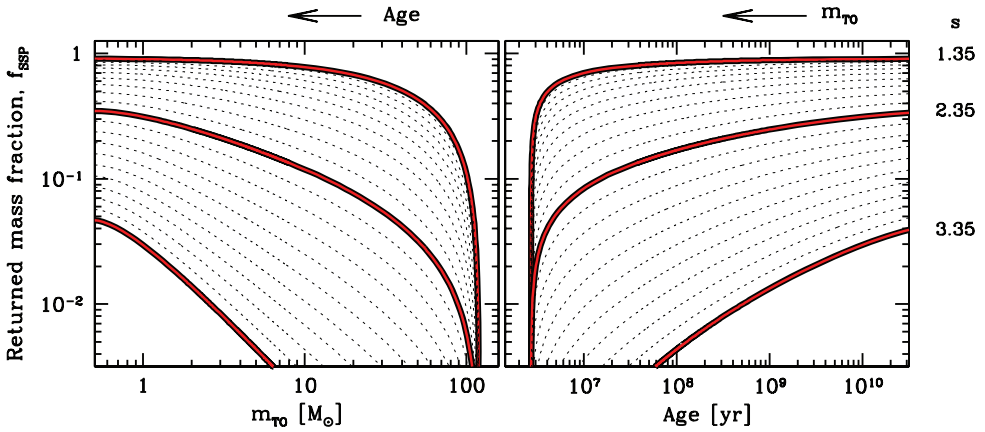

Figure 6. The expected fraction $F_{\rm SSP} = M_{\rm ret}/M_{\rm tot}$ of stellar mass returned to the ISM for a set of SSPs, with changing the IMF power-law index (s), as labelled to the right. The evolution is traced both versus SSP age and the main-sequence Turn Off stellar mass ($m_{\rm TO}$), the latter via equation (3) of Buzzoni (2002). The relevant case for a Salpeter IMF ($s = 2.35$) and two indicative variants for giant- ($s = 1.35$) and dwarf-dominated ($s = 3.35$) SSPs are singled out in both panels, while the thin dotted curves account for the intermediate cases, by steps of $\Delta s = 0.05$ in the IMF index.

3.1.3 The returned mass fraction

The exact knowledge of the way processed stellar mass is returned to the ISM, and the disaggregated contribution of the different elemental species, is clearly the real core of any theoretical effort aiming at tracing the physical details of galaxy chemical evolution. In our straight approach, this concept is fully condensed into returned mass function $f(t)$, which is the ultimate key to quantitatively assess equation (29). The function includes, in principle, a formidable wealth of input physics, dealing with chemical yields for individual stars of different mass, the quiescent and explosive mass-loss properties of stars, the galaxy versus external environment interplay, etc. Such a wide range of ingredients, and their related uncertainties, gives actually reason of the remarkable differences among the Milky Way models reviewed in the previous section.

A very plain, but still instructive, approach to the problem of ISM pollution by returned stellar mass has been investigated by Kennicutt et al. (1994), following the classical scheme of the instantaneous gas recycling extensively practiced in the past literature (see e.g. Larson, Tinsley & Caldwell 1980). Although 'old-fashioned' and evidently inadequate for any detailed assessment of specific elemental abundances (e.g. Arimoto & Yoshii 1986), this method may, however, still accommodate, although with some important refinements, within our analysis for setting a safe upper limit to f. Following the classical treatment (see e.g. Tinsley 1980), we can consider an SSP of total mass $M_{\rm tot}$, and an IMF stellar mass range between 0.1 and 120 $\mathrm{M}_\odot$. With these constraints, the fraction of mass returned to the ISM within the lifetime of Turn Off stars, of mass $m_{\rm TO}$, quantifies in

$$F_{\rm SSP} = \frac{M_{\rm ret}}{M_{\rm tot}} = \frac{(2-s)}{[m^{2-s}]_{0.1}^{120}} \int_{m(TO)}^{120} \Delta_m(m) m^{-s}\, {\rm d}m. \qquad (36)$$

This estimate requires to know the $\Delta_m(m)$ function, that is the mass amount lost by stars of initial mass m, during their post-MS evolution, so that $\Delta_m = m - m_{\rm fin}$. Following the Kennicutt et al. (1994) arguments, we could rely on fully empirical facts, and take the observed Δ_m relation, as from the Galactic open clusters. For example, according to Weidemann (2000), a nice fit can be obtained for stars within the range $0.5\,\mathrm{M}_\odot \lesssim m \lesssim 8\,\mathrm{M}_\odot$, such as

$$\Delta_m = \underset{\pm 4}{0.916}\, m - \underset{\pm 2}{0.44}. \qquad (37)$$

For higher masses, if we assume that a *Chandrasekhar* core of $1.4\,\mathrm{M}_\odot$ is left all the way by the SN events, then

$$\Delta_m = (m - 1.4) \qquad (38)$$

for $m \gtrsim 8\,\mathrm{M}_\odot$. With these figures, the results of our calculations are shown in Fig. 6, exploring the trend of $F_{\rm SSP}$ with varying SSP age or, equivalently, the stellar mass marking the MS Turn Off point of the population. Note that $F_{\rm SSP}$ smoothly increases with SSP age, and for a Salpeter IMF it reaches a 'ceiling' value about $F_{\rm SSP} = 0.32$ after one Hubble time.[11]

On the other hand, as far as a CSP with a more entangled star formation history is concerned, we have to expect the total fraction of returned mass, $F_{\rm CSP}(t)$, to be the result of a convolution with the SFR, such as

$$F_{\rm CSP}(t) = \int_0^t F_{\rm SSP}(\tau) \otimes {\rm SFR}(\tau)\, {\rm d}\tau. \qquad (39)$$

This leads, in general, to a lower value for $F_{\rm CSP}(t)$, compared to the corresponding SSP case. In addition, for a proper assessment of the gas budget in the galaxy one has to also consider that part of the returned mass is in fact to be recycled again into fresh stars, its exact amount being indeed a crucial distinctive property of any theoretical scheme aimed at tracing galaxy chemical evolution. Our conclusion is therefore that, in any case, it must be $f(t) \leq F_{\rm CSP}(t) \leq F_{\rm SSP}(t) \lesssim 0.3$.

3.2 Mixing processes and metallicity spread

One common feature of all these models, however, is that $f(t)$ and the physical conditions that led to establish the galaxy AMR are univocally defined at any epoch. As a consequence, by definition, *no spread in [Fe/H] is envisaged by theory among coeval stars, throughout.* On the other hand, observations of unevolved nearby

[11] One has also to be aware, however, of the extreme sensitivity of this upper limit to the IMF power index, as evident from the curve grid in Fig. 6. A relevant case in this regard is that of a 'diet' Salpeter IMF, as parametrized, for instance, by Kennicutt (1983) or Kroupa, Tout & Gilmore (1993) to better account for the observed flattening in the dwarf-star number counts at sub-solar mass. By means of equation (36) one could verify that this IMF closely traces the standard Salpeter case being, however, capped at a slightly higher value of $F_{\rm SSP} \sim 0.46$.

Downloaded from https://academic.oup.com/mnras/article/415/2/1155/1034920 by INAF –IASF Bologna user on 17 January 2023

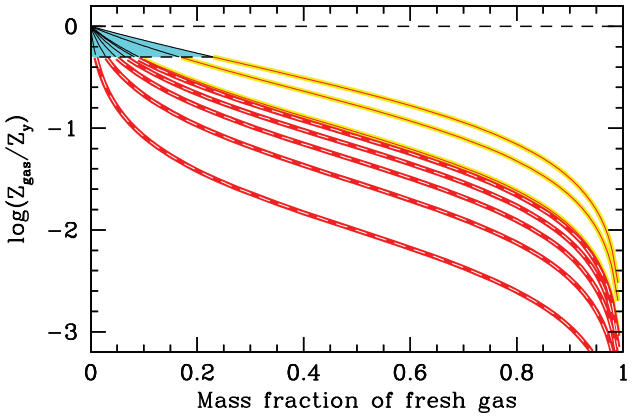

Figure 7. The output of equation (29) is displayed versus the mass fraction of fresh primordial gas ($\mathcal{G}$). The two shelves of curves assume the fraction f of returned stellar mass as a free parameter. The lower shelf (dashed curves) is for $f = 0.01 \rightarrow 0.09$ by steps of $\Delta f = 0.02$, while the upper shelf of curves (solid lines) covers the f range from 0.1 to 0.3, by steps of $\Delta f = 0.1$. The shaded area within $-0.3 \leq \log(Z_{\rm gas}/\mathcal{Z}) \leq 0$ singles out the allowed $f - \mathcal{G}$ combinations that may account for the observed metallicity spread of stars in the solar neighbourhood.

stars clearly point to some degree of metallicity dispersion, perhaps slightly amplified by observational uncertainties and the adopted age/metallicity classification procedure (Rocha-Pinto et al. 2000). For example, by relying on the Edvardsson et al. (1993) survey, we derive σ[Fe/H] = 0.23 dex from the distribution of the individual stars around the mean AMR locus. This is about twice the typical value originally found by Twarog (1980), and can be contrasted with σ[Fe/H] = 0.16 dex, as obtained for the Rocha-Pinto et al. (2000) stars, or with σ[Fe/H] = 0.18 dex, displayed by the Holmberg et al. (2007) extended star sample. Whether this spread is really the general case for spiral galaxies is still an open and debated question (e.g. Koeppen & Arimoto 1990; Wyse 2006; Prantzos 2008).

Again, the envisaged $\mathcal{Z}$ evolution can help, we believe, to set some interesting constraints to this problem, as well. Following equation (29), Fig. 7 summarizes the expected response of the $Z_{\rm gas}/\mathcal{Z}$ ratio to just the two reference parameters that modulate galaxy chemical evolution in our framework, namely $\mathcal{G}$ and f. When regarded into a broader context, our plot displays expected relationship of the global mass fraction of fresh gas in the galaxy. Alternatively, this 'macro' view can be complemented by a 'micro' view, being the $\mathcal{G}$ parameter intended as the local gas density of star-forming regions, such as $\mathcal{G} \equiv \rho_{\rm gas}/\rho_{\rm tot}$, and featuring therefore the specific mixing conditions that embed star formation. One sees from the figure that, in principle, a wide range (a few dex!) may be allowed to $Z_{\rm gas}$, at every epochs, as coeval stars could naturally spread in the plot along an f = const. locus, in consequence of the micro-environment conditions proper to the different star-forming regions inside a galaxy.

The Edvardsson et al. (1993), Rocha-Pinto et al. (2000) and Holmberg et al. (2007) star samples offer once more an important feedback in this regard, as shown in Fig. 8. For the first sample, 161 stars are nominally younger than 13 Gyr, the assumed age of the Milky Way; the overall statistics of their individual Δ[Fe/H] = [Fe/H]$_{\rm yield}$ − [Fe/H]$_*$ distribution indicates that 88 per cent of the stars are comprised within Δ[Fe/H] $\leq$ 0.50 dex, while a fraction of 65 per cent lie within Δ[Fe/H] $\leq$ 0.30 dex. With the same procedure, for the 412 relevant stars in the Rocha-Pinto et al. (2000) sample we obtain a fraction of 97 and 84 per cent, respectively, within

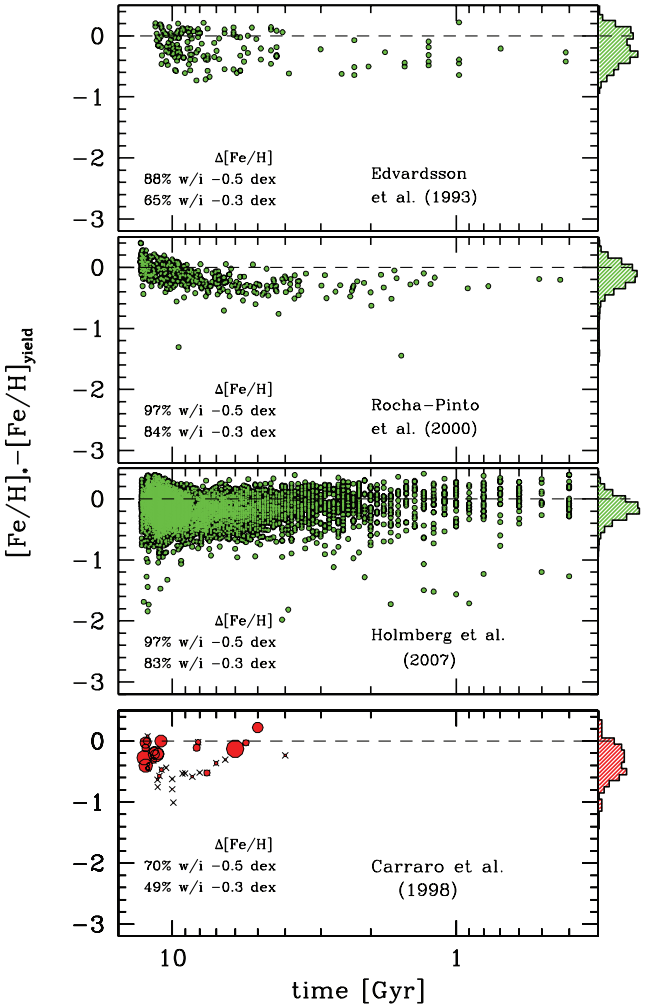

Figure 8. The observed metallicity distribution of stars in the solar neighbourhood. The displayed quantity is Δ[Fe/H] = [Fe/H]$_*$ − [Fe/H]$_{\rm yield}$ ≡ $\log(Z_{\rm gas}/\mathcal{Z})$. Different stellar samples have been considered from the work of Edvardsson et al. (1993), Rocha-Pinto et al. (2000) and Holmberg et al. (2007), from top to bottom, as labelled in each panel. The lower panel displays the same trend for a sample of open stellar clusters, after Carraro, Ng & Portinari (1998). The different Galactocentric distance for these systems is indicatively marked by the dot size (i.e. the smallest the dot, the largest the distance from the Galaxy centre). For each distribution, the relative fraction of stars within a −0.3 and −0.5 dex Δ[Fe/H] residual is reported in each panel. A cumulative histogram of the data is also displayed, along the right axis, in arbitrary linear units.

the same Δ[Fe/H] limits. Similar figures (namely 97 and 83 per cent, respectively) apply also for the 13 141 eligible stars in the Geneva–Kopenhagen catalogue. Overall, this means that over 4/5 of all newly born stars in the solar vicinity never departed by more than 0.3 dex from $\mathcal{Z}$, *at any epoch.*

Facing so tight Δ[Fe/H] ≡ $\log(\mathcal{Z}/Z_{\rm gas})$ star distribution,[12] one may actually wonder *why stars in the Galaxy appear so closely 'tuned' with the yield metallicity, every time.*

[12] Strictly speaking, for its delayed supply to the ISM, iron may not be a fair proxy of the whole metallicity among very metal-poor (i.e. 'pristine') stars in the Galaxy (see Section 3.2.2 for a most explicit assessment of this issue). This assumption carries therefore some uncertainties for stars within $t \lesssim 1$ Gyr in the plots of Fig. 8.

Downloaded from https://academic.oup.com/mnras/article/415/2/1155/1034920 by INAF –IASF Bologna user on 17 January 2023

In spite of any more or less sophisticated approach to this crucial issue, just a glance at Fig. 7 makes evident that the observed range for the $Z_{\rm gas}/\mathcal{Z}$ ratio univocally implies (at least in the solar vicinity) that star formation must have proceeded within ISM conditions characterized, all the way, by *a scanty gas abundance* ($\mathcal{G} \lesssim 0.5$; *see again Fig. 7)*.

Overall, this feature seems to add further strength to well-recognized non-standard scenarios, where the plain dependence of SFR on gas density, like in a classical Schmidt (1959) law, might more effectively be replaced by some positive feedback to other triggering mechanisms, either related to disc dynamical properties, inefficient gas mixing or molecular cloud bunching (Larson & Tinsley 1978; Wyse & Silk 1989; Dopita & Ryder 1994; Oey 2000; Boissier et al. 2003; Scalo & Elmegreen 2004; Nittler 2005; van Zee & Haynes 2006).

A further interesting piece of information can be added to the emerging scenario when probing the Δ[Fe/H] distribution at different Galactocentric distance. This can be done, for instance, by relying on Carraro et al. (1998), who collected homogenous data for a set of 37 open clusters. The evident advantage, in this case, is that age and metallicity can be derived in a more direct way, based on the observed colour–magnitude diagram of the whole stellar members of each cluster.[13] The Carraro et al. (1998) results are reported in the lower panel of Fig. 8, marking the cluster distance from Galaxy centre with a different dot size (i.e. the closer the cluster, the bigger its marker).

The local properties of disc metallicity are consistently traced also by the open cluster population, with a clear additional evidence, however, for less pronounced chemical enhancement processes in the most peripheral stellar systems, for which a systematically larger departure from $\mathcal{Z}$ is displayed in Fig. 8.

3.2.1 *The 'G-dwarf' problem*

In its essence, the tuned distribution of the Δ[Fe/H] parameter, as in the previous discussion, has much to do with the classical 'G-dwarf' problem (van den Bergh 1962; Pagel & Patchett 1975; Twarog 1980), that is an evident lack, nowadays, in the [Fe/H] (or $\log Z$) domain of the 'desired' population of extremely metal-deficient unevolved stars, reminiscent of the earliest evolutionary phases of the disc formation in the Galaxy.

According to our SFR parametrization, for $b \lesssim 0.4$, an expected fraction of $\sim(50 \times 10^6/15 \times 10^9)^b \gtrsim 10$ per cent of G-dwarf stars should have produced in the disc of our galaxy within the lapse ($t \lesssim$ 50 Myr) of the first Type-II SN burst. According to Fig. 2, for these stars a metallicity as poor as [Fe/H] ~ -1.10 should be expected. The lack, nowadays, of such a relevant population of virtually 'zero-metal' stars is actually the central issue that led theorists in the late 80s to invoke a composite formation for the Galaxy disc, through a 'buffering' dynamical mechanism that led first to the formation of an outer 'thin' disc, followed by an inner 'thick' structure (Gilmore & Wyse 1986; Ferrini et al. 1992).

Translated into a linear metallicity scale, the undersized population of stars with [Fe/H] $\ll -1$ can be matched by a roughly uniform star density along the Z range, so that $dN_*/dZ \sim const.$ (see, in this regard, Pagel 1989, and especially the work of Beers, Preston & Shectman 1985, 1992; Sommer-Larsen 1991; Cayrel 1996; Ryan, Norris & Beers 1996).

[13] One has to remark, however, the evident bias of the Carraro et al. (1998) sample against very old open clusters likely due, according to authors' discussion, to the disruptive mechanisms along the past dynamical history of the Galaxy (Friel 1995).

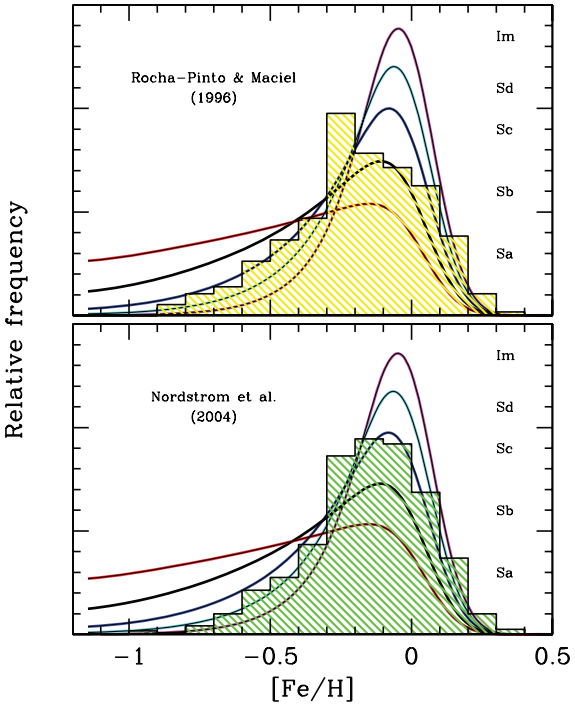

Figure 9. The [Fe/H] distribution of G-dwarf stellar samples in the solar neighbourhood (shaded histograms), according to Rocha-Pinto et al. (2000) (upper panel) and Nordström et al. (2004) (lower panel), is compared with the expected yield–metallicity distribution accounting for the different star formation histories as for the disc stellar population of Buzzoni (2005) template galaxies along the Hubble sequence (solid curves, as labelled on the plot). A roughly constant stellar distribution in the Z domain leads to an implied birthrate of the order of $b \simeq 0.6$, as pertinent to Sbc galaxies (see Table 2 for a reference).

The stellar metallicity distribution can easily be related with the other distinctive properties of galaxy evolution in our framework, as

$$\frac{{\rm d}N_*(Z)}{{\rm d}Z} = \frac{{\rm d}N_*(t)}{{\rm d}t} \Big/ \frac{{\rm d}Z}{{\rm d}t}. \tag{40}$$

The first term in the right hand side of the equation is, of course, proportional to the SFR ($\propto t^{-\beta}$), while the second term is simply the time derivative of the observed AMR ($\propto t^{\zeta-1}$). By replacing the relevant relations, we have

$$\frac{{\rm d}N_*(Z)}{{\rm d}Z} \propto t^{1-\zeta-\beta} \propto Z^{(1-\zeta-\beta)/\zeta}, \tag{41}$$

or

$$\frac{{\rm d}N_*}{{\rm d[Fe/H]}} \propto 10^{[{\rm Fe/H}](1-\beta)/\zeta}, \tag{42}$$

if one better likes to put the relation in terms of [Fe/H]. For a roughly constant dN_*/dZ distribution, it must be $(1-\zeta-\beta) \sim 0$, or $\zeta \simeq b$. According to Table 4, for a current age of 13 Gyr, this implies that G-dwarf distribution may be reproduced by a Galaxy birthrate of

$$b \sim 0.6 \pm 0.1. \tag{43}$$

A graphical sketch of our conclusions is proposed in Fig. 9, by comparing the G-dwarf stellar sample of the Galaxy disc by Rocha-Pinto & Maciel (1996) and Nordström et al. (2004) with

Downloaded from https://academic.oup.com/mnras/article/415/2/1155/1034920 by INAF –IASF Bologna user on 17 January 2023

the expected metallicity distribution as obtained by applying equation (42) for a range of SFR representative of the spiral-galaxy sequence in the Buzzoni (2005) template galaxy models. Note that Milky Way observations closely match the standard case of the Sb/Sc morphological types (see Table 2).

For a better analysis, however, we have to remark the somewhat marginal value of b when compared to our previous conclusions, as the tight relationship between Galaxy AMR and $\mathcal{Z}$ trend rather called for a lower figure (i.e. $b \lesssim 0.4$). This apparent dichotomy actually summarizes the full essence of the G-dwarf problem emphasizing, on the one hand, the central role of the early stellar component in constraining the Galaxy AMR, but requiring, on the other hand, for these stars to be born 'elsewhere' (i.e. in the halo or in the 'thin' disc).

3.2.2 *The 'α'-element versus iron-peak enrichment*

A further implication of the simple energetic arguments outlined in Section 2 is that metal enrichment should have proceeded selectively in the very early stages of Galaxy evolution, according to the composite interplay between 'quiescent' luminosity evolution of stars and violent action of SNe. In fact, bright stars are to be regarded as the elective suppliers of lighter pre-carbon elements, while SNe II further add to the synthesis of the α-element chain, especially providing oxygen and heavier metals (Woosley & Weaver 1995). For their different physical conditions, SNe Ia are meant, on the contrary, to be the prevailing donors of Fe and other iron-peak elements (Nomoto et al. 1984) to the galaxy ISM.

Given the delayed appearance of SN Ia, one has to expect α-elements (and oxygen, in particular) to cumulate earlier than iron-peak elements into ISM of the Milky Way. This feature directly calls, therefore, for some O–Fe decoupling among the low-metallicity stellar component of our galaxy. A positive [O/Fe] relative abundance is actually a widely recognized property when comparing halo and disc stars, and the effect is a supplementary piece of evidence dealing with the G-dwarf problem previously discussed. The study of the [O/Fe] versus [Fe/H] relationship in the local framework prove therefore to set important constraints to the different feeding channels that eventually led to Z enrichment in the Galaxy.

We can further explore this issue by relying on our model to compare the expected [O/Fe] evolution with the observed trend for the Galaxy stars. The work of Pagel & Tautvaisiene (1995) and Scannapieco & Bildsten (2005) can be taken as useful references to set the relevant quantities for Fe and O yields in Type Ia and II SNe. Accordingly, we assume a typical abundance of $[\mathrm{O/Fe}]_{\mathrm{II}} = +0.50$ dex for the released mass by SNe II and $[\mathrm{O/Fe}]_{\mathrm{I}} = -1.51$ dex for the SN Ia case, being $\log(\mathrm{O/Fe})_{\odot} = +1.33$ dex the reference figure (in number abundance) for the Sun (Grevesse & Sauval 1998). In addition, with Scannapieco & Bildsten (2005), we take a ratio $r = (m^{\mathrm{II}}_{\mathrm{Fe}} : m^{\mathrm{Ia}}_{\mathrm{Fe}}) = (0.062 : 0.74)$ for the released iron yields according to the SN type.[14]

Equations (13), (16) and (20) can still accommodate for our calculations providing to replace the $(E_{51}\, 10^{51})/(W_{\mathrm{SN}}\, \mathrm{M}_{\odot})$ energy-release term with the relevant chemical yields. Recalling our SFR parametrization, and the notation of Section 2.2, the total mass

[14] As iron is the main output of any SNIa explosion, its yield must obey an inherent argument of energetic self-consistency being $m^{\mathrm{Ia}}_{\mathrm{Fe}} \approx (E^{\mathrm{SNI}}_{51}\, 10^{51})/(W_{\mathrm{SN}}\, \mathrm{M}_{\odot})$. According to the relevant figures of Section 2.2.2, we actually have that $m^{\mathrm{Ia}}_{\mathrm{Fe}} \simeq 0.75 \pm 0.25\, \mathrm{M}_{\odot}$, in close agreement with the standard model predictions (see e.g. Nomoto et al. 1984, their model W7).

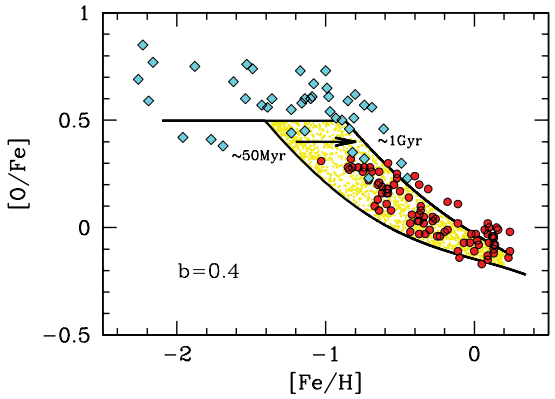

Figure 10. The [O/Fe] distribution of stars in the Milky Way is displayed according to the Jonsell et al. (2005) (diamonds) and Edvardsson et al. (1993) (dots) data samples, respectively, for the halo and disc stellar populations. Our model output, according to equation (46), is superposed (solid lines), for a representative birthrate $b = 0.4$, and for a range of SN Ia delay time Δ from ∼50 Myr to ∼1 Gyr, as discussed in Section 2.2.

released by Type II and Ia SNe for the element X, can be expressed as

$$m(X) = m(X)_{\mathrm{II}} + m(X)_{\mathrm{I}}\, B(t, \Delta, b), \tag{44}$$

where $B(t, \Delta, b)$ is a function of age (t) and stellar birthrate (b), and accounts for the SN Ia delay time (Δ). Like for equation (23), previously discussed, an analytical form can be devised also for this function, providing to express Δ in years, such as

$$B(t, \Delta, b) = \begin{cases} 0 & \text{for } \tau < 1 \\ 0.35\,(1 - \tau^{-b}) + \frac{\Delta}{1.6\times10^{11}}\,\frac{\tau\,[1-\tau^{-(1+b)}]}{1+b}, & \\ & \text{for } \tau \geq 1 \end{cases} \tag{45}$$

being, again, $\tau = t/\Delta$.

For the [O/Fe] relative abundance we have therefore

$$\left[\frac{\mathrm{O}}{\mathrm{Fe}}\right] = \log \frac{r\, 10^{[\mathrm{O/Fe}]_{\mathrm{II}}} + B\, 10^{[\mathrm{O/Fe}]_{\mathrm{I}}}}{r + B} \tag{46}$$

Note, from equation (46), that $B = 0$ for $t \lesssim \Delta$, which implies that ISM [O/Fe] abundance simply coincides with the SN II relative yields at the very early evolutionary stages of the Galaxy. Iron enrichment is obviously favoured by increasing B in the equation. This naturally happens when getting the Galaxy older (i.e. by increasing τ) and/or by decreasing the SN Ia delay time Δ.

Our results are sketched in Fig. 10, comparing with the observation of disc and halo stars, respectively from Edvardsson et al. (1993) and Jonsell et al. (2005). In the figure, a safe lower and upper envelope to the observed [O/Fe] stellar distribution can be placed for $\Delta \sim 50$ Myr and 1 Gyr, respectively. This range also consistently comprises the claimed 'glitch' in the [O/Fe] versus [Fe/H] trend, ideally located about $[\mathrm{Fe/H}] \approx -1$ (Clegg, Tomkin & Lambert 1981). Our output therefore confirms that most of the SN Ia impact on the Galaxy metal enrichment should have occurred very early within the first Gyr of life, although just a glance at the data of Fig. 10 indicates that some 10^8 yr may have required for the SN Ia process to fully deploy within the Galaxy stellar environment. This conclusion is supported, indeed, by the empirical arguments of Maoz et al. (2010) and the theoretical ones by Greggio (2005) and Kobayashi et al. (1998).

Downloaded from https://academic.oup.com/mnras/article/415/2/1155/1034920 by INAF –IASF Bologna user on 17 January 2023

4 CHEMO-PHOTOMETRIC PROPERTIES ALONG THE HUBBLE MORPHOLOGICAL SEQUENCE

Our quite special lookout inside the Galaxy makes the study of our system certainly favoured but, at the same time, also subtly biased, compared to the analysis of external galaxies. On the one hand, in fact, we can directly address the problem of 'Galaxy metallicity' in terms of the aggregated information from individual stars in the solar neighbourhood, and on the other hand the criterion to define the star sample (either by fixed space volume, or apparent magnitude limit, or even selected spectral type, etc.) may play a crucial role in driving our conclusions, as the 'representative' metallicity value would eventually depend on the way we account for the contribution of individual stars. This is a substantial difference with respect to the study of distant galaxies, for which we usually cannot resolve individual stars at all. In the latter case, one should forcedly rely on the integrated spectrophotometric properties of the system, as a whole, to derive somewhat 'effective' distinctive parameters to constrain galaxy properties.

4.1 Matching the Arimoto & Jablonka (1991) theoretical framework

From the theoretical side, our general view of disc chemical properties along the Hubble morphological sequence may usefully complement the analysis of AJ91, certainly one of the few explicit attempts in the recent literature to self-consistently tackle the problem of chemo-photometric evolution of LTGs (see, in addition, also Arimoto & Yoshii 1986, 1987; Koeppen & Arimoto 1990, to complete the theoretical picture). A first interesting comparison, in this regard, is proposed in Fig. 11 where the gas metallicity, $\log(Z_{\rm gas}/Z_{\odot})$, for the 15 Gyr AJ91 disc models along the Sa → Sd sequence is displayed together with the relevant values of our yield metallicity, $\log(\mathcal{Z}/Z_{\odot})$.

For its different IMF limits (stars are produced between 0.05 and 60 $M_{\odot}$) the AJ91 stellar populations are slightly 'darker' (i.e. with a larger M/L ratio) for their larger fraction of dwarf stars, and with a less prominent contribution (~ -20 per cent) of SNe to galaxy metal enrichment. These differences with respect to our theoretical

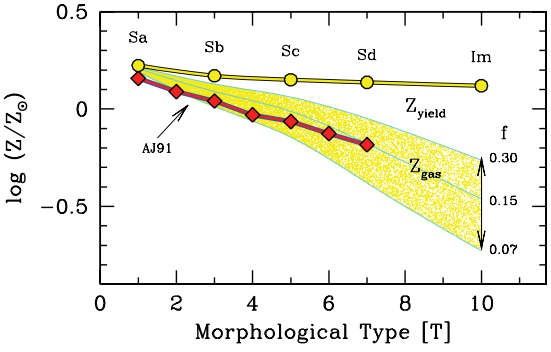

Figure 11. The gas metallicity of 15 Gyr disc stellar populations according to the AJ91 models (solid line with diamonds) is displayed together with the expected predictions from equation (31) (shaded area) for a range of returned mass fraction f between 0.07 and 0.3, as labelled in the plot. For tighter self-consistency in our comparison, the adopted gas fraction $\mathcal{G}_{\rm tot}$ for our model sequence matches the corresponding figures of AJ91 models, while yield metallicity derives from equation (27) for the relevant birthrate values of the Buzzoni (2005) template models along the Sa → Im morphological sequence (solid line with dots).

scheme become more important when moving along the Sa → Sd sequence, as stars of increasingly higher mass prevail as contributors to galaxy luminosity.

In spite of the different input physics, one has to remark, however, a notable agreement in the [Fe/H] predictions, as shown in Fig. 11. The case of Sa models is illustrative in this sense, as the vanishing residual gas (only 4 per cent of the total disc mass in the AJ91 model) makes $Z_{\rm gas}$ to closely approach $\mathcal{Z}$, as expected. Once accounting for the increasing fraction of residual gas along the morphological galaxy sequence, the prediction of equation (31) tightly matches the AJ91 output. Facing the relatively flat trend of $\mathcal{Z}$ versus galaxy type, it is evident from the figure that *the increasingly poorer gas metallicity along the Sa → Im Hubble sequence is in fact mainly the result of the diluting process, that shares enriched stellar mass with a larger fraction of residual gas.*

Interestingly enough, in the quite delicate balancing mechanism that governs the [Fe/H] trend versus Hubble type, the exact details of stellar mass return processes do play a somewhat marginal role. This is evident, for instance, by comparing in Fig. 11 the effect of changing the return mass fraction f from its allowed maximum ($f = 0.3$) down to a factor of 4 lower value ($f = 0.07$). Rather, the amount of fresh residual gas, that survived past star formation, seems a much more central figure to modulate the enrichment process, and this directly calls for the distinctive birthrate b as the ultimate parameter to constrain disc metallicity. We will further return in more detail on this important point in a moment (see Section 4.3).

4.2 'Chemical' versus 'photometric' metallicity estimates

Due to the coexisting contribution of gas and stars inside a spiral galaxy, any fair estimate of 'galaxy metallicity' is a far more entangled problem. Quoting Roberts & Haynes (1994): 'intercomparison between abundances based on emission lines from HII regions and on absorption lines and colors from a stellar population is still uncertain... Atomic processes guide emission-line analysis, while the absorption lines must be evaluated in terms of both the CSP and the metallicity'.

From the observational point of view, the inherent difficulty in disentangling the genuine metallicity effects on the colour properties of LTGs has greatly favoured the alternative approach relying on the study of H II regions as effective proxies of disc metallicity (see e.g. Peimbert, Rayo & Torres-Peimbert 1978; Zaritsky, Kennicutt & Huchra 1994; Peimbert, Carigi & Peimbert 2001; Garnett 2002). Broad-band colours and narrow-band spectrophotometric indices have been imposing, on the contrary, as election tools to probe chemical abundance in the galaxy bulges (Jablonka, Martin & Arimoto 1996; Henry & Worthey 1999; Gorgas, Jablonka & Goudfrooij 2007; Jablonka, Gorgas & Goudfrooij 2007), while they mainly constrain galaxy SFR in the discs (among others, see in particular Kennicutt et al. 1994; Gavazzi 1993; Boselli et al. 2001). In this framework, one remarkable effort towards a photometric approach to the metallicity problem is the work of Pérez, Sánchez-Blázquez & Zurita (2009), providing Lick-index measurements of stellar populations in barred spirals.

An instructive summary of observational galaxy diagnostics is proposed in Fig. 12, where the performance of both 'chemical' (HII regions) and 'photometric' (Lick indices from the aggregated stellar population) methods is compared for a set of spirals along the full Hubble sequence. To the theoretical pattern of Fig. 11, reported as a guideline, we superposed the metallicity estimates for the galaxy set of Zaritsky et al. (1994) (square markers), and for the Pérez et al. (2009) S0/a sample (triangles). As usual, the original

Downloaded from https://academic.oup.com/mnras/article/415/2/1155/1034920 by INAF –IASF Bologna user on 17 January 2023

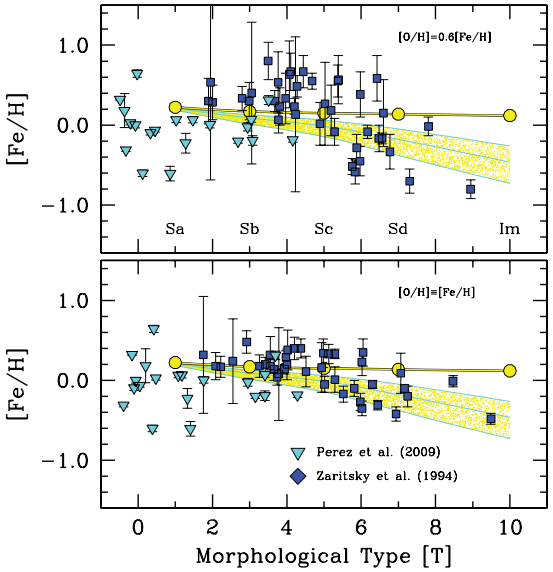

Figure 12. [Fe/H] metallicity for the two galaxy samples of Pérez et al. (2009) (triangles) and Zaritsky et al. (1994) (squares), compared with the yield and gas metallicity figures (solid line with dots and shaded area) as from Fig. 11. While the Pérez et al. (2009) estimates derive from Lick indices tracing the galaxy stellar population, in case of Zaritsky et al. (1994) the [Fe/H] derives from the oxygen abundance of galaxy H II regions, by adopting $\log(\mathrm{O/H})_\odot = 8.83$ for the Sun (Grevesse & Sauval 1998). Two cases are envisaged, in this regard, assuming that oxygen traces iron (and the full metallicity), as in lower panel or, more realistically, that a scale conversion does exist such as [O/H] = 0.6 [Fe/H], as suggested by the observation of disc stars in the Milky Way (Clegg et al. 1981; Bessell et al. 1991; Edvardsson et al. 1993). A little random scatter has been added to the morphological T class of the points in each panel for better reading.

gas metallicity in the Zaritsky et al. (1994) galaxies is given in terms of [O/H] abundance, so that two variants of the figure can be devised, depending whether we plainly assume oxygen to trace global metallicity (so that [O/H] = [Fe/H], as in lower panel of the figure) or, perhaps more realistically, whether decoupled α-element enrichment should be considered to rescale chemical abundance (upper panel), as we have been discussing in the previous section. In the latter case, from different sources (Clegg et al. 1981; Bessell, Sutherland & Ruan 1991; Edvardsson et al. 1993), we set [O/H] = 0.6[Fe/H].

Compared with the theoretical predictions, it is evident from Fig. 12 that any empirical effort to constrain metallicity in spiral galaxies still suffers from very high uncertainty. This is especially evident for the H II measurements of Zaritsky et al. (1994), where point scatter is actually comparable to the claimed internal error of individual measurements. Apparently, this does not seem to be the case for the Pérez et al. (2009) Lick data, although the important point-to-point spread casts evident doubts on the nominal accuracy claimed for the individual [Fe/H] estimates. Definitely, we believe that a σ[Fe/H] $\simeq \pm 0.5$ dex might be regarded as a realistic figure for current empirical (either 'chemical' or 'photometric') estimates of metal abundance in LTG discs.

Once considering in more detail the overlapping range of morphological types between the two galaxy samples in Fig. 12, it is interesting to note that 'photometric' metallicity estimates appear to be systematically lower than 'chemical' estimates. According to our previous arguments, this can be seen as an eloquent example of 'biased' sampling criteria; in fact, by probing gas metallicity we retrieve the current status of galaxy chemical enrichment, while through spectrophotometric Lick indices we are probing the galaxy stellar population 'averaging' along the entire range of age of luminous stars.

4.3 Mass, morphology and birthrate (which drives galaxy metallicity?)

Although morphological classification is the most immediate tool for a 'quick-look' characterization of galaxy properties, it has been long questioned whether morphology univocally seats on intrinsic physical properties of the galaxy system as a whole. This is especially true for LTGs, where the prominent spiral pattern actually involves a relatively small fraction of the galaxian total mass. As extensively discussed in the literature during the last a few decades (Whitford 1962; Roberts & Haynes 1994; Kennicutt 1998), the combined analysis of the galaxy leading properties led to a number of established correlations between 'primary' physical parameters, the most popular one being by far the Tully & Fisher (1977, TF) relation.

On the other hand, the obvious reference role of galaxy *luminosity*, as in the TF relation, can easily be replaced by galaxy *stellar mass*, especially once focusing on galaxy photometric properties in the mid-infrared range, as convincingly demonstrated by Gavazzi (1993). All these different pieces of evidence led eventually to identify galaxy (stellar) mass as (one of) the leading parameters that may intimately mark the life and fate of the spiral systems as a whole (Tully, Mould & Aaronson 1982).

In this framework, the recent ultraviolet study by Marino et al. (2010) may add further interesting arguments to this composite scenario. These authors collected *GALEX* observations of three spiral-rich aggregates, from the Lyon Groups of Galaxies (LGG; Garcia 1993). For their galaxy population, these groups can be regarded as close analogues of the Local Group, displaying a quite 'clean' sample of relatively unperturbed objects seen at comparable distances and covering the whole Hubble morphological sequence. While *GALEX* data allow us to explicitly assess current SFR in these galaxies, the match with long-wavelength magnitudes provide, on the contrary, a more direct hint of the amount of stellar mass, through the appropriate *M/L* conversion ratio.

As a first step of our analysis, galaxy internal extinction has to be sized up relying on the *GALEX* (*FUV* − *NUV*) colour. The latter directly relates to the θ spectral slope of galaxy UV emission assuming, with Calzetti (1999), that $F(\lambda) \propto \lambda^\theta$. The intervening action of dust works in this sense of absorbing stellar luminosity at shorter wavelength making the spectral slope to flatten, so that $\theta \to 0$. On the other hand, population synthesis models (see e.g. Leitherer et al. 1999; Buzzoni 2002) firmly agree in predicting a characteristic spectral slope $\theta_o \simeq -2.1$ in case of any dust-free star-forming activity driven by the presence of high-mass ($M \gtrsim 5\,\mathrm{M}_\odot$) stars. Therefore, the amount of the θ flattening (i.e. $\Delta\theta = \theta - \theta_o$) leads to a straightforward measure of the monochromatic attenuation at the different photometric bands.[15]

Internal reddening appears to be quite high in the UV bands, with the galaxies losing typically 2–3 mag at 1500 Å, a figure which is consistent with the more exhaustive studies of Rifatto, Longo

[15] By adopting the Calzetti (1999) attenuation curve, for the magnitude dimming one derives (cf. e.g. Buzzoni 2002) $A(B) = 1.31\,\Delta\theta$, $A(NUV) = 2.0\,\Delta\theta$ and $A(FUV) = 2.47\,\Delta\theta$, assuming FUV and NUV wavebands to be centred at 1520 Å and 2300 Å, respectively (Neff, Hollis & Offenberg 2008).

Downloaded from https://academic.oup.com/mnras/article/415/2/1155/1034920 by INAF –IASF Bologna user on 17 January 2023

Table 5. Inferred physical properties for the Marino et al. (2010) LGG galaxy sample.

Galaxy ID	Morph type	T	θ	M_B	$\log M^*_{\rm gal}$	$\log {\rm SFR}_o$	b
			LGG 93				
NGC 1249	SBc	6.0	−1.02	−19.57	10.53	0.453	1.07
NGC 1311	SBm	8.8	−1.07	−18.30	9.69	0.009	2.67
IC 1933	Sc	6.1	−1.16	−18.66	10.16	0.226	1.52
IC 1954	SBb	3.2	−0.96	−19.72	10.93	0.423	0.40
IC 1959	SBd	8.4	−1.29	−18.21	9.70	−0.065	2.19
			LGG 127				
NGC 1744	SBcd	6.7	−1.18	−20.24	10.72	0.626	1.04
NGC 1792	SBbc	4.0	−0.24	−22.42	11.91	1.376	0.38
NGC 1800	Sd	8.2	−1.22	−18.78	9.95	0.090	1.77
NGC 1808	SABa	1.2	−0.36	−22.21	12.16	1.035	0.10
NGC 1827	SABc	5.9	−0.22	−19.96	10.70	0.886	1.97
ESO305-009	SBd	8.0	−1.31	−18.39	9.82	−0.022	1.85
ESO305-017	IB	9.9	−1.29	−17.14	9.10	−0.504	3.25
ESO362-011	Sbc	4.2	−2.85	−17.74	10.01	−1.000	0.13
ESO362-019	SBm	8.9	−1.31	−17.72	9.45	−0.314	2.24
			LGG 225				
NGC 3370	Sc	5.1	−1.24	−19.76	10.72	0.207	0.40
NGC 3443	Scd	6.6	−1.18	−17.26	9.54	−0.208	2.32
NGC 3447	Sm	8.8	−1.40	−17.31	9.29	−0.014	6.33
NGC 3447A	IB	9.9	−1.76	−15.15	8.30	−0.768	11.0
NGC 3454	SBc	5.5	−0.62	−19.08	10.39	−0.209	0.32
NGC 3455	SABb	3.1	−0.73	−18.31	10.37	0.434	1.48
NGC 3501	Sc	5.9	−0.78	−18.99	10.31	−0.142	0.45
NGC 3507	SBb	3.1	−1.07	−20.10	11.09	0.422	0.28
UGC 6022	I	9.9	−1.31	−14.87	8.19	−1.127	6.27
UGC 6035	IB	9.9	−1.27	−16.48	8.83	−0.695	3.82
UGC 6083	Sbc	4.1	−0.82	−17.39	9.88	−0.722	0.32
UGC 6112	Scd	7.4	−1.04	−17.49	9.54	−0.248	2.12
UGC 6171	IB	9.9	−1.60	−16.36	8.78	−0.847	3.02

Notes. Morphological-type classification from the Marino et al. (2010) compilation; spectral slope θ from $(FUV - NUV)$ colour as $\theta = -[2 + 0.4\,(FUV - NUV)/\log(1520/2300)]$; absolute B magnitude M_B from B_T from RC3 (de Vaucouleurs et al. 1991), except UGC 6022, which is from UGC (Nilson 1973), after correction for reddening (see footnote 15) and distance, the latter derived from the mean redshift of the parent group, assuming a pure Hubble flow with $H_o = 75\,{\rm km\,s^{-1}\,Mpc^{-1}}$; galaxy stellar mass in $\mathrm{M}_\odot$ from M/L_B, according to Buzzoni (2005); SFR in $\mathrm{M}_\odot\,{\rm yr^{-1}}$ from the dereddened NUV flux, according to footnote 16; birthrate b assumes a current galaxy age of 13 Gyr.

& Capaccioli (1995) and Gordon, Calzetti & Witt (1997). Once accounted for reddening and distance, UV absolute luminosities directly translate into actual ${\rm SFR}_o$,[16] while absolute B magnitude can eventually relate to galaxy stellar mass ($M^*_{\rm gal}$) through the appropriate M/L ratio from the Buzzoni (2005) template galaxy models, as in Table 2. The galaxy characteristic birthrate can also be computed from our data, as $b = {\rm SFR}_o t_o / M^*_{\rm gal}$, by assuming $t_o = 13$ Gyr.

The results of our analysis are collected in Table 5, and are summarized in Fig. 13. Just as a reference, in each panel of the figure we also reported the typical error figures of the data (see the ellipses in each plot); in particular, we estimate a ± 0.2 dex uncertainty on the inferred value of $\log {\rm SFR}_o$ (mainly as a consequence of the inherent uncertainty on the value of θ), and a ± 0.2 dex uncertainty for the derived galaxy mass (accounting for the reddening uncertainty and M/L calibration). This eventually leads to a $\Delta \log b = \pm 0.3$ dex for our birthrate estimates.

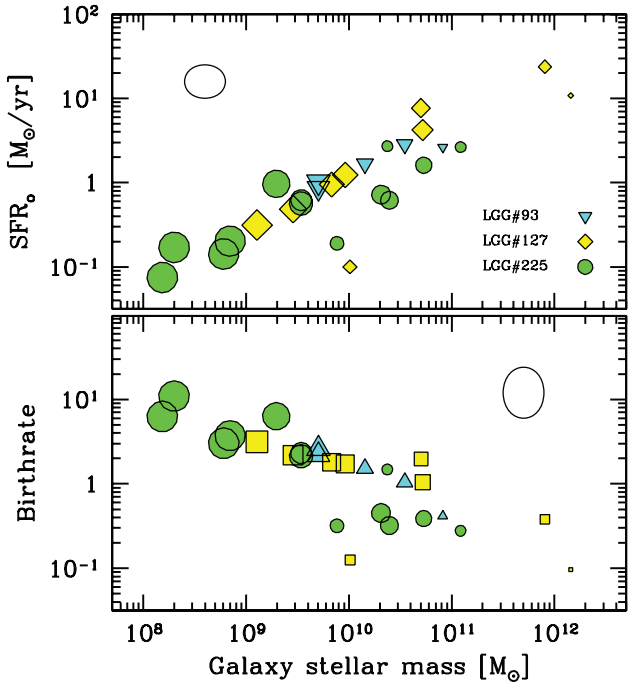

Figure 13. The inferred star formation properties of the spiral-galaxy sample by Marino et al. (2010), referring to three Local-Group Analogues from the LGG catalogue (Garcia 1993), as marked and labelled on the plot. Marker size indicates galaxy morphology along the RC3 T-class sequence (the biggest markers are for Sd/Im galaxies with $T \sim 10$, while the smallest are for Sa systems with $T \sim 1$). Current SFR derives from *GALEX* NUV fluxes, dereddened as discussed in the text, and calibrated according to Buzzoni (2002). On the contrary, Galaxy stellar mass is computed from the relevant M/L_B ratio, as from the Buzzoni (2005) template galaxy models. The birthrate assumes for all galaxies a current age of 13 Gyr. The small ellipses in each panel report the typical uncertainty figures, as discussed in the text. All the relevant data for this sample are summarized in Table 5. Note the inverse relationship between b and $M^*_{\rm gal}$, as in the down-sizing scenario for galaxy formation.

From both plots, a nice correlation ($\rho = 0.86$) is in place between star formation properties and galaxy (stellar) mass. Indeed, the agreement might even be better if one could compare consistently with the *disc* stellar mass alone.[17]

A nominal fit to the data in the upper panel of Fig. 13 provides

$$\log {\rm SFR}_o = \underset{\pm 7}{0.56} \log M^*_{\rm gal} - \underset{\pm 7}{5.6} \qquad [\mathrm{M}_\odot\,{\rm y^{-1}}] \tag{47}$$

with $\sigma(\log {\rm SFR}_o) = \pm 0.31$ dex. As, by definition, ${\rm SFR}_o \propto b M^*_{\rm gal}$, the deviation from the one-to-one slope implies a dependence of the

[16] According to Buzzoni (2002), the inferred SFR (in $\mathrm{M}_\odot\,{\rm yr^{-1}}$) from *GALEX* NUV luminosities is $\log {\rm SFR} = \log F_{Galex} + 27.70$, providing to express flux density, in $\mathrm{erg\,s^{-1}\,Hz^{-1}}$. This calibration is for a Salpeter IMF with stars between 0.1 and 120 $\mathrm{M}_\odot$.

[17] While the UV emission mainly traces star formation activity in the galaxy *disc*, our stellar mass derives, on the contrary, from the integrated B magnitudes, thus including the bulge photometric contribution. For this reason, especially for Sa/b spirals, the value of $\log M^*_{\rm gal}$ may be overestimating the disc mass up to a factor of ∼4 (cf. table 3 of Buzzoni 2005), thus leading also to a correspondingly lower value of b.

Downloaded from https://academic.oup.com/mnras/article/415/2/1155/1034920 by INAF –IASF Bologna user on 17 January 2023

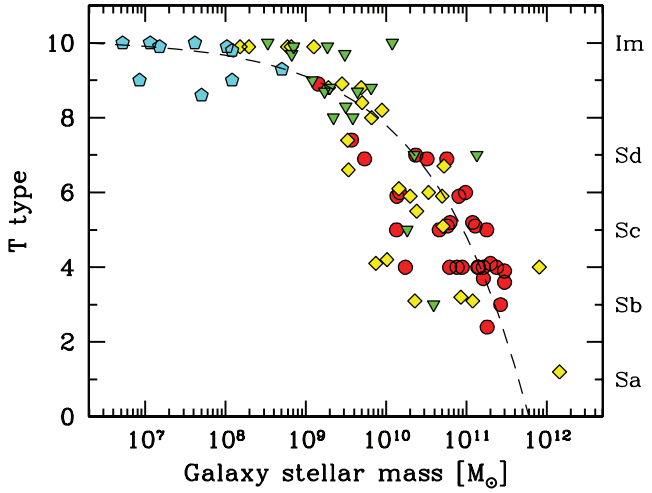

Figure 14. The observed relationship between morphological RC3 class T and galaxy stellar mass according to four different galaxy samples from the work of Garnett (2002) (dots), Marino et al. (2010) (diamonds), Kuzio de Naray et al. (2004) (triangles) and Saviane et al. (2008) (pentagons) (see Tables 5 and 6 for details). The value of $M^*_{\rm gal}$ derives from B photometry for the Garnett (2002), Kuzio de Naray et al. (2004) and Marino et al. (2010) galaxies, and from H absolute magnitudes for the Saviane et al. (2008) sample, through the appropriate M/L ratio, according to Buzzoni (2005). Equation (49) provides a fair representation of the data, as displayed by the dashed curve. As already pointed out also by Roberts & Haynes (1994) one has to remark, however, the notable dispersion in mass among Sbc galaxies.

birthrate on the galaxy mass such as

$$b \propto M_{\rm gal}^{-0.44}, \tag{48}$$

as confirmed, indeed, by the point distribution in the lower panel. In its essence, the inverse correlation of birthrate with galaxy mass closely deals with the nowadays recognized effect of 'down-sizing' (Cowie et al. 1996; Gavazzi, Pierini & Boselli 1996), the imposing paradigm in theory of galaxy formation.

The claimed link with galaxy morphology is another issue to be considered. In this case, however, a poorer correlation ($\rho = 0.59$) readily appears for the same data as far as the SFR_o distribution versus the RC3 classification type 'T' is dealt with. This is partly in consequence of a less tuned relationship between galaxy mass and morphological type, as shown in Fig. 14. In addition to the Marino et al. (2010) galaxies, we also joined to the figure the sample of standard spirals studied by Garnett (2002), complemented by the low-surface-brightness galaxy sample of Kuzio de Naray, McGaugh & de Blok (2004), and the dI collection by Saviane et al. (2008). For the different sets of data we derived $M^*_{\rm gal}$ with a similar procedure as for the Marino et al. (2010) data, namely based on the integrated B (for Garnett 2002; Kuzio de Naray et al. 2004) and H luminosity (for Saviane et al. 2008), respectively. Again, a global fit to the data can be adjusted, tentatively in the form:

$$T = 10.1 - \left(M^*_{\rm gal}/10^9\right)^{0.36}. \tag{49}$$

While the general trend is evident from the data ($\rho = 0.83$), one could easily verify that any attempt to use equation (49) for predicting galaxy morphology based on the mass, alone, is a nearly hopeless task.[18] In particular, to a closer analysis, one has to report that grand-design spirals (type Sbc or class $T \sim 4$) seem to

[18] The rms of the equation (49) fit can be written as $\sigma(T) \sim (8\text{–}0.8\,T)$.

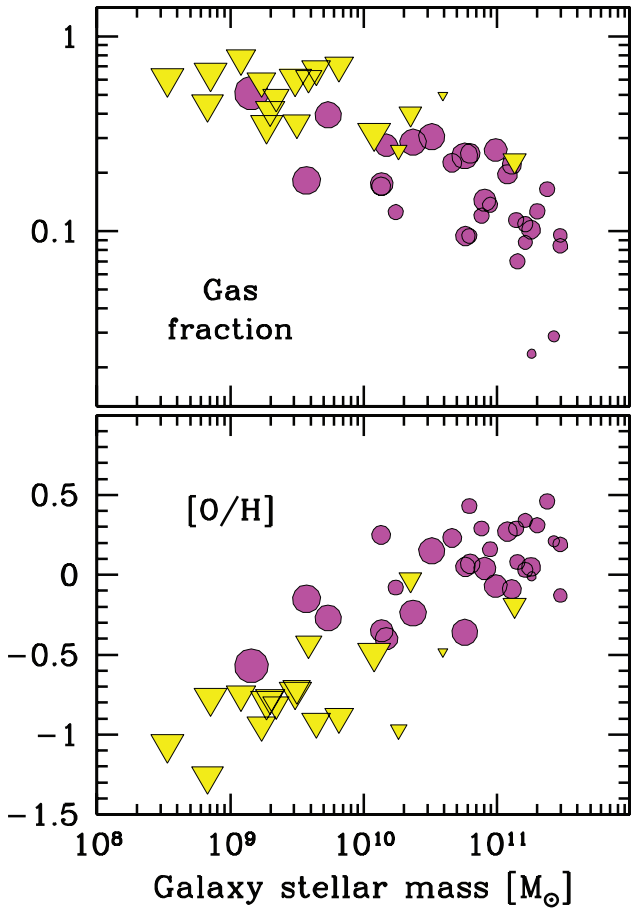

Figure 15. Mass fraction of gas and oxygen abundance of HII regions for the Garnett (2002) (dots) and Kuzio de Naray et al. (2004) (triangles) galaxy samples of Table 6. Marker size is propotional to the galaxy morphological class T (the biggest markers are for Sd/Im galaxies with $T \sim 10$, while the smallest are for Sa systems with $T \sim 1$). Gas fraction accounts for both atomic and molecular phase. Note the inverse relationships of the data versus galaxy stellar mass, the latter as derived from the relevant M/L ratio (see, again, Table 6 for details).

set along a wider spread of mass (nearly 2 dex in $\log M^*_{\rm gal}$), a feature that partially blurs the otherwise cleaner T–mass relationship, as already pointed out by Roberts & Haynes (1994). Moreover, this picture cannot easily accommodate even dwarf ellipticals, that however seem to markedly characterize the high-density cosmic environment (Cellone & Buzzoni 2005; Gavazzi et al. 2010). As is well known, both these features directly call for a longstanding quest in the extragalactic debate about the role of primordial genesis and the environment 'nurture' to modulate galaxy morphology (e.g. Dressler 1980; Thuan, Balkowski & Tran Thanh Van 1992; Blanton et al. 2005; Cooper et al. 2007; Tasca et al. 2009).

As far as galaxy metallicity is concerned, an interesting picture can be devised, relying again on the Garnett (2002) and Kuzio de Naray et al. (2004) contributions. In Fig. 15, we further elaborated their original data displaying, in the two panels, the mass fraction of fresh gas (including atomic and molecular hydrogen), and the representative [O/H] abundance of HII regions. For the reader's better convenience, a summary of these data is also reported in Table 6. The gas fraction $\mathcal{G}_{\rm tot} = M_{\rm gas}/(M_{\rm gas} + M^*_{\rm gal})$ can easily be

Downloaded from https://academic.oup.com/mnras/article/415/2/1155/1034920 by INAF –IASF Bologna user on 17 January 2023

derived from the data in force of the tight $M_{\rm gas}/M^*_{\rm gal}$ relationship:

$$\log M_{\rm gas} = \underset{\pm 8}{0.60}\ \log M^*_{\rm gal} + \underset{\pm 87}{3.51}, \qquad (50)$$

with $\sigma(\log M_{\rm gas}) = \pm 0.25$ dex and $\rho = 0.81$.

The upper panel of the figure shows the somewhat unescapable consequence of the enhanced birthrate among low-mass systems. A higher value of b implies that a larger fraction of fresh gas must still be available at present time. Actually, one may even speculate that such a delayed mass processing is in fact the natural explanation also of the low-metallicity figures that characterize, all the way, the dwarf-galaxy population in the Universe (Arimoto & Tarrab 1990; Lee, Grebel & Hodge 2003). This scenario seems to find direct support once exploring, as in the upper panel of Fig. 16, H II metallicity over the whole range of galaxy mass, for instance by extending again the Garnett (2002) sequence for 'standard' spirals with the low-mass samples of Kuzio de Naray et al. (2004) and Saviane et al. (2008) (see also Table 6).

On the other hand, a far more instructive experiment can be carried out with the help of equation (31). Facing a change of the reference value for the gas fraction, $\mathcal{G}_{\rm tot}$, the equation allows us to compute the induced change in the value of $Z_{\rm gas}$, by accounting for the different ISM dilution factor. Accordingly, the observed gas metallicity could easily be rescaled to any other reference value of $\mathcal{G}_{\rm ref}$ starting from the observed value of $\mathcal{G}_{\rm obs}$. As far as the HII metallicity is considered, the expected offset to the observed [O/H] abundance can therefore be written as

$$\Delta[{\rm O/H}] = \log\left(\frac{1-\mathcal{G}_{\rm ref}}{\mathcal{G}_{\rm ref}}\right) - \log\left(\frac{1-\mathcal{G}_{\rm tot}}{\mathcal{G}_{\rm tot}}\right). \qquad (51)$$

By entering equation (51) with the values of $\mathcal{G}_{\rm tot}$ from Table 6 we can eventually rescale galaxy metallicity to the same reference gas fraction, say for example $\mathcal{G}_{\rm ref} = 0.2$, such as $[{\rm O/H}]_{0.2} = [{\rm O/H}]_{\rm obs} + \Delta[{\rm O/H}]$. The result of our exercise is shown in the lower panel of Fig. 16 for the joint sample of galaxies.

Definitely, once accounting for the increasing fraction of fresh gas with decreasing galaxy mass, one sees that *most of the observed trend of [O/H] with $M^*_{\rm gal}$ may simply be recovered by the dilution effect of processed mass on the ISM.*

4.4 The Roberts time and the fate of spiral galaxies

As discussed in Section 2.1, the rate at which the mass is chemically enriched inside a galaxy follows a sort of universal law; calculations show in fact that the burning efficiency factor, $\mathcal{F}$ (see Table 1), is nearly insensitive to the galaxy star formation history. At present, about 11 ± 2 per cent of the processed mass in galaxies has been converted into heavy elements and, according to equation (8), the process may go ahead for a supplementary factor of $(0.11)^{-1/0.23} \sim 10^4$ of the Hubble time.[19] At that time, hydrogen will definitely vanish even inside stars, and a maximum metallicity $Z_{\rm max}$ has to be reached by the system for $(1 + R)Z_{\rm max} = 1 - Y_{\rm p}$. In terms of the solar figures, galaxy chemical evolution will eventually end

[19] Curiously enough, the matter annihilation that accompanies nuclear burning processes may also result, in the long term, in a not quite negligible effect for the total mass budget of a galaxy. Previous figures show, for instance, that the Milky Way has already lost in luminosity about one thousandth (i.e. a factor of 0.11×0.0078; see footnote 2) of its total mass. This is roughly the equivalent mass of the whole globular-cluster system currently surrounding our galaxy.

Table 6. Inferred physical properties for the Garnett (2002), Kuzio de Naray et al. (2004) and Saviane et al. (2008) galaxy samples.

Galaxy ID	Morph. type[a]	$\log M^*_{\rm gal}$ ($M_\odot$)	$\mathcal{G}^b_{\rm tot}$	[O/H][c]	$[{\rm O/H}]^d_{0.2}$
		Garnett (2002)			
NGC 224	3.0	11.44	0.03	0.21	−0.72
NGC 253	5.1	10.80	0.09	0.05	−0.33
NGC 300	6.9	9.95	0.40	−0.27	0.15
NGC 598	5.9	10.22	0.17	−0.35	−0.42
NGC 628	5.2	10.92	0.25	0.07	0.20
NGC 925	7.0	10.52	0.29	−0.24	−0.04
NGC 1232	5.0	11.30	0.10	0.05	−0.29
NGC 1637	5.0	10.21	0.17	0.25	0.16
NGC 2403	6.0	10.31	0.28	−0.40	−0.22
NGC 2442	3.7	11.25	0.09	0.34	−0.08
NGC 2805	6.9	10.88	0.24	−0.36	−0.25
NGC 2903	4.0	10.83	0.09	0.43	0.05
NGC 3031	2.4	11.27	0.02	−0.01	−1.03
NGC 3344	4.0	10.30	0.13	−0.08	−0.32
NGC 3521	4.0	10.94	0.12	0.29	0.03
NGC 3621	6.9	10.67	0.31	0.15	0.40
NGC 4254	5.2	11.17	0.20	0.27	0.26
NGC 4258	4.0	11.18	0.07	0.08	−0.44
NGC 4303	4.0	11.26	0.11	0.03	−0.28
NGC 4321	4.1	11.36	0.13	0.31	0.07
NGC 4395	8.9	9.47	0.51	−0.57	0.05
NGC 5033	5.1	11.22	0.22	−0.09	−0.04
NGC 5055	4.0	11.01	0.14	0.16	−0.04
NGC 5194	4.0	11.20	0.11	0.29	0.00
NGC 5236	5.0	10.77	0.22	0.23	0.29
NGC 5457	6.0	11.12	0.26	−0.07	0.08
NGC 6384	3.6	11.52	0.10	−0.13	−0.51
NGC 6744	4.0	11.45	0.16	0.46	0.36
NGC 6946	5.9	10.97	0.14	0.04	−0.13
NGC 7331	3.9	11.51	0.08	0.19	−0.25
NGC 7793	7.4	9.66	0.18	−0.15	−0.20
		Kuzio de Naray et al. (2004)			
F563-1	8.0	9.34	0.49	−0.81	−0.23
F571-5	9.0	9.08	0.77	−0.75	0.38
UGC 1230	8.7	9.64	0.68	−0.92	0.01
UGC 5005	9.9	9.27	0.35	−0.79	−0.46
UGC 9024	3.0	10.59	0.50	−0.48	0.12
UGC 12695	8.8	9.81	0.71	−0.89	0.10
F415-3	9.9	8.85	0.65	−0.77	0.10
F469-2	8.7	9.23	0.59	−0.94	−0.18
F530-3	5.0	10.26	0.26	−0.97	−0.82
F561-1	8.3	9.50	0.36	−0.71	−0.36
F563-V1	9.7	8.83	0.45	−1.26	−0.75
F563-V2	9.7	9.49	0.61	−0.73	0.07
F568-6	7.0	11.13	0.23	−0.19	−0.11
F577-V1	8.0	9.59	0.61	−0.43	0.37
F611-1	10.0	8.53	0.61	−1.06	−0.26
F746-1	10.0	10.08	0.32	−0.49	−0.22
UGC 5709	7.0	10.35	0.40	−0.03	0.40
UGC 6151	8.8	9.30	0.42	−0.77	−0.31
		Saviane et al. (2008)			
ESO 347-G017	9.0	8.08	*0.67*	−0.91	0.00
UGC A442	8.6	7.70	*0.74*	−1.11	−0.05
ESO348-G009	10.0	7.62	*0.76*	−0.83	0.27
NGC 59	−3.0	8.31	*0.62*	−0.76	0.06
ESO473-G024	10.0	7.06	*0.84*	−1.33	−0.01
AM0106-382	9.0	6.93	*0.85*	−1.18	0.19
NGC 625	9.3	8.70	*0.54*	−0.75	−0.08

Downloaded from https://academic.oup.com/mnras/article/415/2/1155/1034920 by INAF –IASF Bologna user on 17 January 2023

Table 6 – *continued*

Galaxy ID	Morph. type[a]	log $M^*_{\rm gal}$ ($M_\odot$)	$\mathcal{G}^b_{\rm tot}$	[O/H][c]	$[{\rm O/H}]^d_{0.2}$
ESO245-G005	9.9	8.02	*0.68*	−0.91	0.03
DDO42	9.8	8.08	*0.67*	−1.08	−0.17
DDO53	9.9	7.18	*0.82*	−0.91	0.36
UGC4483	10.0	6.72	*0.88*	−1.30	0.15

[a]Morphological class T, as reported by HyperLeda (Paturel et al. 2003).
[b]Gas fraction $\mathcal{G}_{\rm tot} = M_{\rm gas}/(M_{\rm gas} + M^*_{\rm gal})$; for the Saviane et al. (2008) sample $\mathcal{G}$ is extrapolated from equation (50).
[c]For the Sun we assume $\log({\rm O/H})_\odot = 8.83$ (Grevesse & Sauval 1998).
[d][O/H] abundance rescaled to $\mathcal{G}_{\rm tot} = 0.2$.

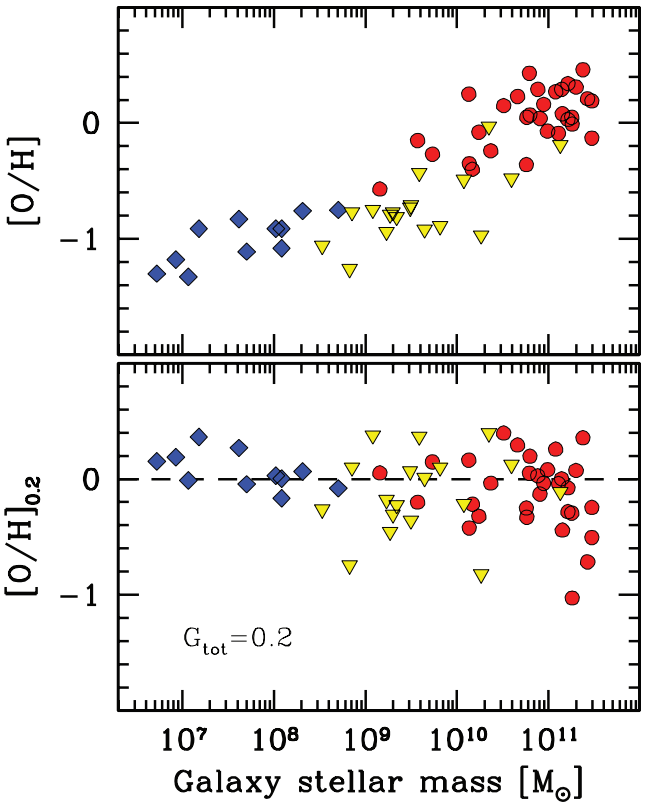

Figure 16. Upper panel: oxygen abundance from H II regions for the galaxy samples of Garnett (2002) (dots), Kuzio de Naray et al. (2004) (triangles) and Saviane et al. (2008) (diamonds). A nice correlation is in place with galaxy stellar mass, where low-mass systems appear richer in gas (see Fig. 15) and poorer in metals. Once accounting for the different gas fraction among the galaxies, and rescaling oxygen abundance to the same gas fraction ($G_{\rm tot} = 0.2$, as in the indicative example displayed in the lower panel), note that most of the [O/H] versus $M^*_{\rm gal}$ trend is recovered, leaving a nearly flat [O/H] distribution along the entire galaxy mass range, as predicted by the nearly constant yield metallicity of the systems.

up with

$$(Y_{\rm max}, Z_{\rm max}) \simeq (3\,{\rm Y}_\odot, 10\,{\rm Z}_\odot). \quad (52)$$

On the other hand, much earlier than the full process completion, other outstanding events could mark the chemical history of a galaxy. In particular, if one recalls that $\mathcal{S} \propto t^b$, and takes the Hubble time ($t_{\rm H}$) as a reference, then the expected evolution of the fresh-gas content in the disc scales as

$$\frac{(1-\mathcal{G})}{(1-\mathcal{G}_{\rm H})} = \left(\frac{t}{t_{\rm H}}\right)^b. \quad (53)$$

If we set $\mathcal{G} = 0$ and recall equation (30), then the time-scale for the galaxy to consume its primordial-gas reservoir is

$$t_{\rm R} = \frac{t_{\rm H}}{(1-\mathcal{G}_{\rm H})^{1/b}} = t_{\rm H}\left(\frac{1-f}{1-\mathcal{G}_{\rm tot}}\right)^{1/b}, \quad (54)$$

$\mathcal{G}_{\rm tot}$ and f evaluated at the (current) Hubble time. After a $t_{\rm R}$ time, the so-called 'Roberts time' (Roberts 1963), star formation can only proceed further in a galaxy at the cost of exploiting its own processed mass. Since long, the problem of a realistic estimate of the Roberts time-scale has been investigated (Sandage 1986; Kennicutt et al. 1994), leading to the quite puzzling conclusion that $t_{\rm R}$ may not substantially depart from one Hubble time. As a consequence, present-day galaxies might be all on the verge of exhausting their own gas resources. To overcome this somewhat embarrassing conclusion, it has been emphasized that, after all, even at time $t_{\rm R}$ a galaxy is not completely gas depleted, still counting on a residual buffer $M_{\rm gas} \simeq f\,M^*_{\rm gal}$ of processed mass (see equation 31) still rich in hydrogen and able, in principle, to sustain galaxy SFR for the Gyr to come (Kennicutt 1998).

We can take advantage of our original approach to galaxy chemo-photometric evolution to attempt a more confident assessment of the Roberts time, also in its 'extended' definition ($t_{\rm Re}$), such as to account for the 'extra-time' provided by processed-mass recycling. First of all, according to its standard definition, the value of $t_{\rm R}$ can easily be computed with our data along the different galaxy mass by means of equation (50). Once getting the value of $M_{\rm gas}$ from the fitting equation, it is immediate to derive $\mathcal{G}_{\rm tot} = M_{\rm gas}/(M_{\rm gas} + M^*_{\rm gal})$. Galaxy birthrate follows, as well, by relying on equation (47), and recalling that $b \simeq {\rm SFR_H}\,t_{\rm H}/M^*_{\rm gal}$. The results of equation (54) are displayed in Fig. 17, maintaining the net value of the returned mass fraction (f) as a free parameter in our calculations. Evidently, the current evolutionary scenario can typically be sustained by spiral galaxies only for a further 20 per cent of the Hubble time. For the most massive systems this is 2–3 Gyr ahead from now.

When returned stellar mass is included in our budget too, then fresh stars can still form for a supplementary time lapse such as to lead to $\mathcal{G}_{\rm tot} = 0$. Recalling again, equation (30), then the 'extended' Roberts time ($t_{\rm Re}$), follows from equation (53) as

$$t_{\rm Re} = \frac{t_{\rm H}}{(1-\mathcal{G}_{\rm tot})^{1/b}} = \frac{t_{\rm R}}{(1-f)^{1/b}}, \quad (55)$$

again with $\mathcal{G}_{\rm tot}$ and f referring to the boundary conditions of present-day galaxies (see Fig. 17). Two important conclusions can be drawn from the analysis of these results.

(i) For any realistic assumption about the returned mass fraction, *most of the galaxies more massive than* $\sim 10^{11}\,{\rm M}_\odot$ *have* $t_{\rm R} \lesssim t_{\rm H}$. *As a consequence, they may already have exceeded their Roberts time, being their current SFR mainly driven by processed mass rather than by primordial gas.* According to the morphology versus mass relationship (see again Fig. 14) this seems to be the case for most of the Sa/Sb spirals in the present-day Universe.

(ii) When explicitly included in the gas budget, the processed-mass contribution certainly adds supplementary chances to high-mass spirals for continuing their star formation activity for a few Gyr. However, the relative life extension is critically constrained by the balance of the two antagonic processes of mass return (f) and mass consumption (b). In absolute terms, equation (55) shows that the 'extended' Roberts time, $t_{\rm Re}$, is eventually driven by the 'down-sizing' mechanism, which constrains the b versus mass relationship. *The conclusion is that only a marked reduction of the present birthrate might allow spirals to sustain star formation far beyond one Hubble time.* In any case, only a negligible 'bonus'

Downloaded from https://academic.oup.com/mnras/article/415/2/1155/1034920 by INAF –IASF Bologna user on 17 January 2023

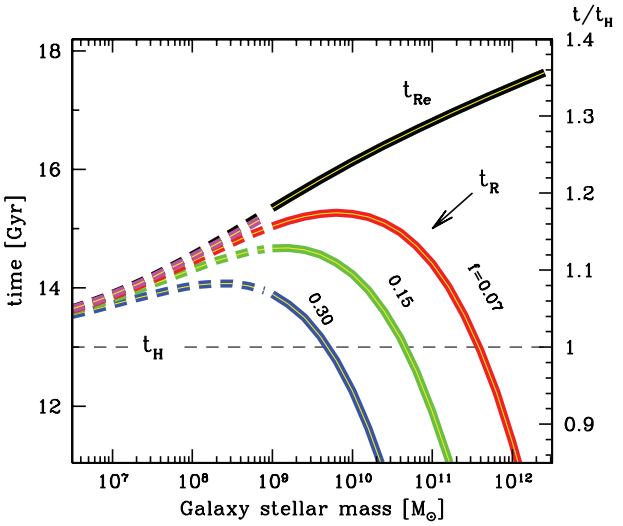

Figure 17. The lifetime of spiral galaxies as active star-forming systems, better recognized as the Roberts (1963) time, is computed along the full mass range of the systems. The definite consumption of the primordial gas reservoir, as in the original definition of the time-scale, t_R, derives from equation (54), by parametrizing with the current fraction of returned stellar mass, f. Present-day galaxies are assumed to be one Hubble time old ($t_H \sim$ 13 Gyr; see the left scale on the vertical axis). If returned stellar mass is also included in the fuel budget, to further extend star formation, the 'extended' Roberts time, t_{Re}, derives from equation (55). In both equations, the distinctive birthrate relies on the observed down-sizing relationship of equation (47), while the gas fraction available to present-day galaxies is assumed to obey equation (50), eventually extrapolated for very low mass systems (i.e. $M^*_{gal} \lesssim 10^9\,M_\odot$) (dashed curves in the plot). Note, for the latter, that they seem on the verge of definitely ceasing their star formation activity, while only high-mass galaxies ($M^*_{gal} \gtrsim 10^{11}\,M_\odot$) may still have chance to extend their active life for a supplementary 30-40 per cent lapse of t_H. See text for a full discussion.

is awarded to low-mass systems (namely to Sd/Im galaxies less massive than $\sim 10^{11}\,M_\odot$). For them, in fact, we definitely have $t_{Re} \simeq t_R \simeq t_H$, and just a couple of Gyr, at most, still seem to be left ahead.

5 SUMMARY AND CONCLUSIONS

In this paper, we tried an alternative approach to the study of chemo-photometric properties of LTGs. Following previous theoretical efforts in this sense (e.g. Pagel 1997), our analysis relies on a basic criterion of energetic self-consistency between chemical enhancement of galaxy mass through nuclear processing and the corresponding luminosity evolution of the system.

This plain physical constraint provides us with a brand new interpretative tool, as nearly all the leading theoretical codes along the last decades rather approached the problem of galaxy chemical evolution in terms of the sum of individual elemental contributions (see e.g. Tinsley 1980). This required, in other words, to explicitly account for the chemical yields supplied by stars along the different range of mass. Clearly, this 'analytical' approach is the unescapable way when we want to trace the specific enrichment history of single chemical elements. On the other hand, as far as the global metallicity of a stellar aggregate is concerned, the analytical process risks to carry along and magnify the combined uncertainty from stellar evolution theory making the emerging picture to strongly depend on the model assumptions, often through a plethora of free tunable parameters.

On the contrary, in any 'synthetic' approach, galaxy chemical evolution derives from other primary physical constraints. The work of Schmidt (1963) and Pagel & Patchett (1975) are two outstanding examples in this sense, assessing the chemical history of a stellar system as an *implied consequence* of its star formation law. As a further variant on this line, our reasoning takes the move from the fact that a fixed amount of energy must always be released when matter is chemically enhanced through nuclear processing inside stars. Theoretical nucleosynthesis predicts, in fact, that 6.98×10^{18} erg are produced (see Section 2) for each gram of hydrogen to be converted to heavier elements through non-explosive burning processes. A further amount of 1.03×10^{18} erg per gram should then be added if we want to account for the explosive nucleosynthesis dealing with the SN events. Overall, it is clear that a tight relationship has therefore to be expected between chemical enhancement of a galaxy and its past photometric history.

The theoretical fundamentals which provide the reference framework for our analysis have been discussed in Section 2. In particular, we rely on the Buzzoni (1989, 1995) original code for stellar population synthesis, further elaborated to build up three-zone galaxy templates along the Hubble morphological sequence (Buzzoni 2002, 2005). For its special relevance within the global properties of late-type systems, our study is mainly focused on the disc evolution, which broadly marks the macroscopic look of spiral and irregular galaxies. The standard scenario of the present calculations considers a Salpeter IMF, with stars formed within a mass range between 0.1 and $120\,M_\odot$. In addition, metals and helium proceed from processed stellar mass assuming a fixed enrichment ratio $R = 3$, as discussed in Section 2.3.

Following Buzzoni (2005), an important assumption of our models is that stellar birthrate is a distinctive property of galaxy morphology and mass (the latter, in force of the observed T–M^*_{gal} relationship, as shown in Fig. 14). Consistent with the downsizing scenario for galaxy formation (Cowie et al. 1996), b is therefore seen to decrease, in our models, with increasing M^*_{gal} (Gavazzi 1993). As a consequence, SFR scales with time according to a power law, and it is not directly coupled to the mean gas density of the disc as imposed, on the contrary, by other classical schemes (Schmidt 1959).

Chemical enhancement inside a galaxy is effectively assessed by the burning efficiency factor, as displayed in equation (8) of Section 2.1. Table 1 reports a notable property of $\mathcal{F}$, being nearly insensitive to the galaxy star formation history. Along a full range of possible evolutionary scenarios, in fact, we always end up at present time with $\mathcal{F} = 0.11 \pm 0.02$. This means, in other words that, within just small (± 20 per cent) individual differences, galaxies performed very similarly everywhere in the Universe as efficient engines for energetic exploitation of the barionic matter through nuclear synthesis. Accordingly, at any epoch we can univocally define a reference figure, which we called 'yield metallicity' ($\mathcal{Z}$; see equation 24 in Section 2.3), which traces the mean composition of the stellar mass.

The role of SNe in the more general context of disc chemical evolution has been assessed in some detail in Section 2.2. A comparison of the energetic budget involved in quiescent and explosive nucleosynthesis indicates that SNe are extremely powerful mass processors; for fixed amount of released energy, in fact, they burn a factor of 7 more mass than 'normal' stars. Following classical arguments (e.g. Matteucci & Greggio 1986), we know that the component of high-mass stars ($M \gtrsim 5\,M_\odot$) enables a very quick chemical enrichment during early evolution of galaxies. This 'prompt' chemical enhancement is the result of the explosion of both core-collapsed

Downloaded from https://academic.oup.com/mnras/article/415/2/1155/1034920 by INAF –IASF Bologna user on 17 January 2023

objects, in the form of Type II SNe, and accreted WDs as a result of binary interactions, like in Type Ia SNe.

Yield metallicity is therefore abruptly raised to $\log \mathcal{Z} \sim -3$ on a time-scale of a few 10^7 yr, a figure that further increases by $\sim$0.15 dex within the first Gyr of galaxy life (see Fig. 2). As, by definition, the cumulative action of 'prompt' SNeII and Ia must be proportional to the galaxy stellar mass $M^*_{\rm gal}$, the net effect of their contribution is to set a *steady offset* (that we quantified in Section 3.2 in [Fe/H] $\simeq -1.10$ dex) to galaxy yield metallicity.

In this framework, for a Salpeter IMF, the implied yield metallicity evolves as $\mathcal{Z} \propto t^{0.23}$ (see equation 25). For the previous arguments, this can be seen as a nearly universal law, only marginally dependent on the galaxy birthrate (see e.g. Fig. 3). An immediate consequence of this important property is that IMF, rather than SFR, is the key player to set metallicity at primeval epochs, when $t \rightarrow 0$ and SNe were governing chemical evolution (e.g. Scannapieco, Schneider & Ferrara 2003). In particular, non-Salpeter stellar populations, strongly biased towards high-mass stars as in a flatter IMF, have to be invoked to fit with the peculiar presence of bright super-solar galaxies at high redshift, as sometimes observed (e.g. Maiolino et al. 2006) and also envisaged by some updated theoretical schemes (see e.g. the interesting explorations of Kroupa & Weidner 2003; Köppen, Weidner & Kroupa 2007). Fig. 1 is an illustrative example of this mechanism when tracing the contribution of SNeII to metal enhancement with varying the IMF power-law index.

A major advantage of taking yield metallicity as a reference marker in our analysis is that $\mathcal{Z}$ can easily be related to other key physical processes that constrain galaxy chemical evolution in its different facets. The ISM metal enrichment is an evident example in this sense. Chemical composition of the gaseous phase inside a galaxy is the resulting balance of two basic mechanisms. On the one hand, one should carefully consider the bulk of processed mass returned by stars to the ISM through SN events and quiescent stellar wind. On the other hand, this input has to be properly assessed in the physical context of dynamical evolution of the disc, such as to trace the way processed mass is eventually 'diluted' within the fresh primordial gas.

In tackling the problem (Section 3.1), we tried to maintain our formal treatment as much as possible free from any *'ab initio'* assumptions that might bias our conclusions. The returned mass flow is therefore dealt with in equation (28) in terms of the parametrized fraction $f(t)$ of net stellar mass returned to the ISM within the time t (see footnote 10). In our notation, this component is always traced separately from the primordial gas component $\mathcal{G}(t)$, so that the global gas amount in the disc comes throughout as a sum of the two nominal contributions, as in equation (30). In its formal elaboration (see equations 29 and 31), the ISM metallicity ($Z_{\rm gas}$) can eventually be set in terms of yield metallicity, and derives from just two leading parameters, namely $\mathcal{G}$ and f (see Fig. 7). For the latter, a safe upper limit has been placed, such as $f \lesssim 0.3$ at any age for a Salpeter IMF, according to a full discussion of the SSP case, as in Section 3.1.3.

The case of the Milky Way must be the obvious and preeminent test bed for our theoretical framework. In particular, the expected evolution of the yield metallicity is compared, in Fig. 4, with the observed AMR, as traced by different stellar samples in the solar neighbourhood. By definition, at every epoch $\mathcal{Z}$ caps the value of the ISM metallicity, and therefrom edges the composition of newly formed stars. As discussed in Section 3.1, the study of the Δ[Fe/H] $\simeq \log(Z_{\rm gas}/\mathcal{Z})$ difference is rich, full of important information to constrain the Galaxy star formation history. We have been able, for instance, to set a firm upper limit to the Galaxy birthrate, such as $b \lesssim 0.5$ (see equation 33), while the current contribution of the primordial gas cannot exceed roughly one-third of the local mass density of the disc (see equation 35). A further boundary condition can also be posed to the chemical enrichment ratio, that must be $R \lesssim 5$.

A similar comparison, performed between 'analytical' model predictions from several reference codes in the literature and observed AMR, is summarized in Fig. 5. The broad range of envisaged scenarios predicted by theory leads to a spread of up to 0.5 dex in the value of stellar [Fe/H] at a given age. We want to look at this figure as a measure of the intrinsic limit of theory to master the combined interplay among the many leading mechanisms that modulate chemical evolution. To a closer analysis, however, it has to be recognized a clear tendency of models to predict a sharper chemical evolution of Galaxy disc, such as to exceed, in most cases, the observed stellar metallicity at the present epoch. Evidently, the shallower enrichment rate indicated by the observations points to a still unsettled problem with the primeval steps of disc evolution, and more specifically with the pre-enrichment processes related to the well-known G-dwarf problem. It is interesting to see, in this regard, that when the observed stellar [Fe/H] distribution is explicitly dealt with in our analysis, as in Section 3.2.1, the implied birthrate ($b = 0.6 \pm 0.1$) tends to oversize the corresponding figure derived from the AMR. Such a more 'delayed' star formation is in fact a sign for primeval stars to have formed 'elsewhere' (alias in the 'thin' disc, as claimed by the standard established scenario).

An outstanding dyscrasia of any theoretical scheme for Galaxy chemical evolution is that no spread in [Fe/H] can be admitted among coeval stars populating the same region of the system, being the AMR univocally settled by the boundary physical conditions of the model. This is evidently at odds with what we observe, at least in the solar neighbourhood, where an intrinsic σ[Fe/H] up to 0.2 dex seems an unquestionable feature for the local stellar population (see Fig. 8). As an important consequence of the metal dispersion, one may actually conclude that, disregarding age, about four out of five stars in the solar vicinity approach the expected yield metallicity within a factor of 2. When interpreted in terms of mixing properties between enriched and primordial gas, such a tuned distribution clearly demonstrates that star formation in the Galaxy only proceeded, all the time, in a highly contaminated environment. This claim can be better quantified by means of Fig. 7, which confirms that the processed stellar mass returned to the ISM must in fact be the prevailing component to gas density in star-forming regions if we want [Fe/H] of fresh stars at any epoch to closely match (i.e. within Δ[Fe/H] $\simeq 0.3$ dex) the yield metallicity, as observed.

This evidence severely tackles the classical scheme *à la Schmidt*, where the star formation strength is fully driven by just the mean gas density. On the contrary, what might be the real case is that the star formation process in spiral galaxies behaves like a wild 'outbreak', that stems from previously contaminated regions to progressively spread across the rest of galaxy body (Nepveu 1988, 1989; Barnes 2004).

The possible implication of the Milky Way scenario to the more general case of LTG evolution along the Hubble morphological sequence has been the focus of Section 4. As far as the close by external galaxies in the local Universe are concerned, observations still hamper any firm assessment of galaxy metal abundance. As a matter of fact (see Fig. 12), the galaxy-to-galaxy scatter of [Fe/H] distribution seems to largely overcome the nominal accuracy of any individual estimate, a feature that makes evident the intrinsic difficulty in defining a fair 'representative' metallicity when such

Downloaded from https://academic.oup.com/mnras/article/415/2/1155/1034920 by INAF –IASF Bologna user on 17 January 2023

a composite stellar environment is dealt with, as in the LTG discs (AJ91).

On the other hand, the combined study of the other leading parameters can add important information that greatly help in constraining the problem. In this regard, our discussion along Section 4.3 basically grounds on three relevant relationships that emerge from the observational properties of different galaxy samples. In particular, they are as follows.

(i) The down-sizing mechanism appears to govern star formation in the local Universe, as well, with a clear relationship between current SFR and galaxy stellar mass (see Fig. 13).

(ii) The 'delayed' star formation among low-mass galaxies, as implied by the inverse $b - M^*_{\rm gal}$ dependence, naturally leads to a more copious gas fraction when moving from giant to dwarf galaxies, as observed indeed (see Fig. 15).

(iii) The physical relationship of star formation mechanisms with galaxy stellar mass can also approximately fit into a straight morphological scheme (Fig. 14), where galaxies with decreasing mass more likely take the look of later-type spirals. It has to remain clear, however, that mass *not* morphology is the primary parameter that govern LTG properties (Boselli et al. 2001).

Once accounting for galaxy chemical properties, by taking for instance oxygen abundance of HII regions as a tracer, the blurring trend with morphology leaves space to a much cleaner relationship with galaxy stellar mass, as in the upper panel of Fig. 16. Facing the fact that low-mass systems also appear richer in gas and poorer in metals, one might even speculate on a simple scenario where the observed trend is in fact merely the result of the softening mechanism that leads enriched stellar mass to mix into fresh unprocessed gas in the ISM. Actually, when galaxy data are properly rescaled to a fixed reference value of $\mathcal{G}_{\rm tot}$, through equation (51), one sees (lower panel of Fig. 16) that most of the [O/H] versus $M^*_{\rm gal}$ trend is recovered, leaving a nearly flat [O/H] distribution along the entire galaxy mass range. This result is consistent with our theoretical predictions for a nearly constant yield metallicity along the entire LTG sequence.

Striking evidence, when sampling the local Universe, is that spiral galaxies appear all dangerously close to shut down their venture as stars forming systems, being on the verge of exhausting their own gas resources. A so-special case, and our somewhat suspicious temporal location as privileged observers, did not escape the analysis of many authors in the literature, leading Roberts (1963) first to wonder about the real 'residual life' left to spiral systems according to their current gas capabilities. Relying on our notation, the so-called Roberts time ($t_{\rm R}$) easily derives in its original definition, namely as the time-scale for the primordial gas to vanish (see equation 54). On the other hand, and more interestingly, one would like to assess the even more general case, when the global gas consumption (i.e. including returned stellar mass) eventually sets (or overcome) the ultimate limit to galaxy star formation (Kennicutt et al. 1994).

Equation (55) shows that, as far as the down-sizing prescriptions set the reference relationship between birthrate and galaxy mass, one has to conclude that spiral galaxies cannot escape an age where no stars will form at all. In fact, if returned mass is left as the only gas supplier to the ISM, then the maximum birthrate that a galaxy can sustain is of the order of $b_{\rm max} \simeq \dot{f}\, t_{\rm H}/(1-f) \ll f/(1-f)$, which must evidently be much less than $\sim$0.45, for a Salpeter IMF. As a result, only massive ($M_{\rm gal} \gtrsim 10^{11}\,{\rm M}_\odot$) Sa/Sb spirals may have some chance to extend their active life for a while (namely for $\sim 0.3\, t_{\rm H}$, as indicated by Fig. 17). On the contrary, no way out seems to be envisaged for dwarf systems, that will soon cease their star formation activity unless to drastically reduce their apparent birthrate below the $b_{\rm max}$ figure.

ACKNOWLEDGMENTS

I would like to thank Luis Carrasco and Peppo Gavazzi for so many inspiring discussions along all these years, when gazing together at stars and galaxies atop the Mexican mountains. Thanks are also due to Robert Kennicutt, for his wise comments to the draft of this paper, and to Giovanni Carraro and Ivo Saviane, for their warm hospitality during my visit at the ESO premises in Santiago de Chile, where part of this work was been conceived. Finally, the anonymous referee is especially acknowledged for a number of very constructive suggestions, which greatly helped better focus the key issues of the paper.

This work has made extensive use of different online extragalactic databases, namely the NASA/IPAC Extragalactic Data base (NED), operated by JPL/CIT under contract with NASA, the Hyper-Linked Extragalactic Databases and Archives (HyperLeda) based at the Lyon University and the VizieR catalogue service of the Centre de Données astronomiques de Strasbourg. Part of the data retrieval has been eased by the DEXTER graphic interface, hosted at the German Astrophysical Virtual Observatory (GAVO) in Heidelberg.

REFERENCES

Alibés A., Labay J., Canal R., 2001, A&A, 370, 1103
Arimoto N., Jablonka P., 1991, A&A, 249, 374 (AJ91)
Arimoto N., Tarrab I., 1990, A&A, 228, 6
Arimoto N., Yoshii Y., 1986, A&A, 164, 260
Arimoto N., Yoshii Y., 1987, A&A, 173, 23
Baade W., 1944, ApJ, 100, 137
Barnes J. E., 2004, MNRAS, 350, 798
Beers T. C., Preston G. W., Shectman S. A., 1985, AJ, 90, 2089
Beers T. C., Preston G. W., Shectman S. A., 1992, AJ, 103, 1987
Bessell M. S., Sutherland R. S., Ruan K., 1991, ApJ, 383, L71
Blanton M. R., Eisenstein D., Hogg D. W., Schlegel D. J., Brinkmann J., 2005, ApJ, 629, 143
Boissier S., Prantzos N., 1999, MNRAS, 307, 857
Boissier S., Prantzos N., Boselli A., Gavazzi G., 2003, MNRAS, 346, 1215
Boselli A., Gavazzi G., Donas J., Scodeggio M., 2001, AJ, 121, 753
Brandt T. D., Tojeiro R., Aubourg É., Heavens A., Jimenez R., Strauss M. A., 2010, AJ, 140, 804
Buzzoni A., 1989, ApJS, 71, 817
Buzzoni A., 1995, ApJS, 98, 69
Buzzoni A., 2002, AJ, 123, 1188
Buzzoni A., 2005, MNRAS, 361, 725
Calzetti D., 1999, Mem. Soc. Astron. Italiana, 70, 715
Carigi L., 1994, ApJ, 424, 181
Carlberg R. G., Dawson P. C., Hsu T., Vandenberg D. A., 1985, ApJ, 294, 674
Carraro G., Ng Y. K., Portinari L., 1998, MNRAS, 296, 1045
Casagrande L., Flynn C., Portinari L., Girardi L., Jimenez R., 2007, MNRAS, 382, 1516
Cayrel R., 1996, Astron. Astrophys. Rev., 7, 217
Cellone S. A., Buzzoni A., 2005, MNRAS, 356, 41
Chevalier R. A., 1976, Nat, 260, 689
Chiappini C., Matteucci F., Gratton R., 1997, ApJ, 477, 765
Clayton D. D., 1983, Principles of Stellar Evolution and Nuclear Nucleosynthesis. Univ. of Chicago Press, Chicago
Clegg R. E. S., Tomkin J., Lambert D. L., 1981, ApJ, 250, 262
Cooper M. C. et al., 2007, MNRAS, 376, 1445
Cowie L. L., Songaila A., Hu E. M., Cohen J. G., 1996, AJ, 112, 839

Downloaded from https://academic.oup.com/mnras/article/415/2/1155/1034920 by INAF –IASF Bologna user on 17 January 2023

Dahlen T. et al., 2004, ApJ, 613, 189
Dallaporta N., 1973, A&A, 29, 393
de Vaucouleurs G., de Vaucouleurs A., Corwin H. G., Jr, Buta R. J., Paturel G., Fouque P., 1991, Third Reference Catalog of Bright Galaxies. Springer, Heidelberg
Dopita M. A., Ryder S. D., 1994, ApJ, 430, 163
Dressler A., 1980, ApJ, 236, 351
Edvardsson B., Andersen J., Gustafsson B., Lambert D. L., Nissen P. E., Tomkin J., 1993, A&A, 275, 101
Ferrini F., Matteucci F., Pardi C., Penco U., 1992, ApJ, 387, 138
Firmani C., Tutukov A., 1992, A&A, 264, 37
Flynn C., Holmberg J., Portinari L., Fuchs B., Jahreiß H., 2006, MNRAS, 372, 1149
Friel E. D., 1995, ARA&A, 33, 381
Fukugita M., Kawasaki M., 2006, ApJ, 646, 691
Garcia A. M., 1993, A&AS, 100, 47
Garnett D. R., 2002, ApJ, 581, 1019
Gavazzi G., 1993, ApJ, 419, 469
Gavazzi G., Pierini D., Boselli A., 1996, A&A, 312, 397
Gavazzi G., Fumagalli M., Cucciati O., Boselli A., 2010, A&A, 517, 73
Giavalisco M. et al., 2004, ApJ, 600, L103
Gilmore G., Wyse R. F. G., 1986, Nat, 322, 806
Giovagnoli A., Tosi M., 1995, MNRAS, 273, 499
Gordon K. D., Calzetti D., Witt A. N., 1997, ApJ, 487, 625
Gorgas J., Jablonka P., Goudfrooij P., 2007, A&A, 474, 1081
Greggio L., 1997, MNRAS, 285, 151
Greggio L., 2005, A&A, 441, 1055
Greggio L., Renzini A., 1983, A&A, 118, 217
Grevesse N., Sauval A. J., 1998, Space Sci. Rev., 85, 161
Hashimoto M., 1995, Prog. Theor. Phys., 94, 663
Henry R. B. C., Worthey G., 1999, PASP, 111, 919
Hillebrandt W., Niemeyer J. C., Reinecke M., Travaglio C., 2003, Mem. Soc. Astron. Italiana, 74, 942
Holmberg J., Nordström B., Andersen J., 2007, A&A, 475, 519
Jablonka P., Martin P., Arimoto N., 1996, AJ, 112, 1415
Jablonka P., Gorgas J., Goudfrooij P., 2007, A&A, 474, 763
Jonsell K., Edvardsson B., Gustafsson B., Magain P., Nissen P. E., Asplund M., 2005, A&A, 440, 321
Kasen D., Plewa T., 2007, ApJ, 662, 459
Kennicutt R. C., Jr, 1983, ApJ, 272, 54
Kennicutt R. C., Jr, 1998, ARA&A, 36, 189
Kennicutt R. C., Jr, Tamblyn P., Congdon C. E., 1994, ApJ, 435, 22
Khokhlov A., Mueller E., Hoeflich P., 1993, A&A, 270, 223
Kobayashi C., Tsujimoto T., Nomoto K., Hachisu I., Kato M., 1998, ApJ, 503, L155
Koeppen J., Arimoto N., 1990, A&A, 240, 22
Köppen J., Weidner C., Kroupa P., 2007, MNRAS, 375, 673
Kroupa P., Weidner C., 2003, ApJ, 598, 1076
Kroupa P., Tout C. A., Gilmore G., 1993, MNRAS, 262, 545
Kuzio de Naray R., McGaugh S. S., de Blok W. J. G., 2004, MNRAS, 355, 887
Larson R. B., 1976, MNRAS, 176, 31
Larson R. B., Tinsley B. M., 1978, ApJ, 219, 46
Larson R. B., Tinsley B. M., Caldwell C. N., 1980, ApJ, 237, 692
Lee H., Grebel E. K., Hodge P. W., 2003, A&A, 401, 141
Leitherer C. et al., 1999, ApJS, 123, 3
Lequeux J., Peimbert M., Rayo J. F., Serrano A., Torres-Peimbert S., 1979, A&A, 80, 155
Maciel W. J., 2001, Ap&SS, 277, 545
Maeder A., 1992, A&A, 264, 105
Maiolino R. et al., 2006, Mem. Soc. Astron. Italiana, 77, 643
Mallik D. C. V., Mallik S. V., 1985, J. Astrophys. Astron., 6, 113
Mannucci F., Della Valle M., Panagia N., Cappellaro E., Cresci G., Maiolino R., Petrosian A., Turatto M., 2005, A&A, 433, 807
Maoz D., Sharon K., Gal-Yam A., 2010, ApJ, 722, 1879
Marigo P., Chiosi C., Kudritzki R.-P., 2003, A&A, 399, 617
Marino A., Bianchi L., Rampazzo R., Buson L. M., Bettoni D., 2010, A&A, 511, A29
Matteucci F., 2003, The Chemical Evolution of the Galaxy, Astrophysics & Space Science Library. Kluwer Academic Publ., Dordrecht
Matteucci F., 2004, in McWilliam A., Rauch M., eds, Origin and Evolution of the Elements, from the Carnegie Obs. Centennial Symp., Cambridge Univ. Press, Cambridge, p. 85
Matteucci F., François P., 1989, MNRAS, 239, 885
Matteucci F., Greggio L., 1986, A&A, 154, 279
Matteucci F., Recchi S., 2001, ApJ, 558, 351
Melchior A.-L., Combes F., Gould A., 2007, A&A, 462, 965
Meusinger H., Stecklum B., Reimann H.-G., 1991, A&A, 245, 57
Mihara K., Takahara F., 1996, PASJ, 48, 467
Miller G. E., Scalo J. M., 1979, ApJS, 41, 513
Milone L. A., Milone A. A. E., 1988, Ap&SS, 150, 299
Neff S. G., Hollis J. E., Offenberg J. D., 2008 'Galex Observer's Guide', Web edition available online at http://galexgi.gsfc.nasa.gov/docs/galex/Documents
Nepveu M., 1988, A&A, 193, 173
Nepveu M., 1989, A&A, 224, 86
Nilson P., 1973, Uppsala General Catalogue of Galaxies, Acta Universitatis Upsalienis, Nova Regiae Societatis Upsaliensis, Series v
Nittler L. R., 2005, ApJ, 618, 281
Nomoto K., 1980, in Type I Supernovae, Proc. Texas Workshop. Univ. of Texas, Austin, p. 164
Nomoto K., Thielemann F.-K., Yokoi K., 1984, ApJ, 286, 644
Nordström B. et al., 2004, A&A, 418, 989
Oey M. S., 2000, ApJ, 542, L25
Pagel B. E. J., 1989, in Beckman J. E., Pagel B. E. J., eds, Evolutionary Phenomena in Galaxies. Cambridge Univ. Press, Cambridge, p. 201
Pagel B. E. J., 1997, Nucleosynthesis and Chemical Evolution of Galaxies. Cambridge Univ. Press, Cambridge
Pagel B. E. J., Patchett B. E., 1975, MNRAS, 172, 13
Pagel B. E. J., Tautvaisiene G., 1995, MNRAS, 276, 505
Pagel B. E. J., Simonson E. A., Terlevich R. J., Edmunds M. G., 1992, MNRAS, 255, 325
Panagia N., Della Valle M., Mannucci F., 2007, in Antonelli L. A., et al., eds, AIP Conf. Proc. Vol. 924, The Multicolored Landscape of Compact Objects and Their Explosive Origins. Am. Inst. Phys., New York, p. 373
Pardi M. C., Ferrini F., 1994, ApJ, 421, 491
Paturel G., Petit C., Prugniel P., Theureau G., Rousseau J., Brouty M., Dubois P., Cambrésy L., 2003, A&A, 412, 45
Peimbert M., Rayo J. F., Torres-Peimbert S., 1978, ApJ, 220, 516
Peimbert M., Carigi L., Peimbert A., 2001, Ap&SS, 277, 147
Peimbert A., Peimbert M., Luridiana V., 2002, ApJ, 565, 668
Pérez I., Sánchez-Blázquez P., Zurita A., 2009, A&A, 495, 775
Pilyugin L. S., Edmunds M. G., 1996, A&A, 313, 783
Portinari L., Chiosi C., Bressan A., 1998, A&A, 334, 505
Prantzos N., 2008, in Charbonnel C., Zahn J.-P., eds, EAS Pub. Ser., Vol. 32, Stellar Nucleosynthesis: 50 Years after B^2FH. p. 311
Prantzos N., Aubert O., 1995, A&A, 302, 69
Reinecke M., Hillebrandt W., Niemeyer J. C., 2002, A&A, 386, 936
Renzini A., Buzzoni A., 1983, Memorie della Societa Astronomica Italiana, 54, 739
Renzini A., Buzzoni A., 1986, Aptrophys. Space Sci. Libr., 122, 195
Rifatto A., Longo G., Capaccioli M., 1995, A&AS, 114, 527
Roberts M. S., 1963, ARA&A, 1, 149
Roberts M. S., Haynes M. P., 1994, ARA&A, 32, 115
Rocha-Pinto H. J., Maciel W. J., 1996, MNRAS, 279, 447
Rocha-Pinto H. J., Maciel W. J., Scalo J., Flynn C., 2000, A&A, 358, 850
Romano D., Chiappini C., Matteucci F., Tosi M., 2005, A&A, 430, 491
Ryan S. G., Norris J. E., Beers T. C., 1996, ApJ, 471, 254
Salpeter E. E., 1955, ApJ, 121, 161
Sandage A., 1986, A&A, 161, 89
Sandage A., Fouts G., 1987, AJ, 93, 74
Saviane I., Ivanov V. D., Held E. V., Alloin D., Rich R. M., Bresolin F., Rizzi L., 2008, A&A, 487, 901
Scalo J., Elmegreen B. G., 2004, ARA&A, 42, 275
Scannapieco E., Bildsten L., 2005, ApJ, 629, L85
Scannapieco E., Schneider R., Ferrara A., 2003, ApJ, 589, 35

Downloaded from https://academic.oup.com/mnras/article/415/2/1155/1034920 by INAF –IASF Bologna user on 17 January 2023

Schmidt M., 1959, ApJ, 129, 243
Schmidt M., 1963, ApJ, 137, 758
Serrano A., Peimbert M., 1981, Rev. Mex. Astron. Astrofis., 5, 109
Smartt S. J., Eldridge J. J., Crockett R. M., Maund J. R., 2009, MNRAS, 395, 1409
Sommer-Larsen J., 1991, MNRAS, 249, 368
Sullivan M. et al., 2006, ApJ, 648, 868
Tasca L. A. M. et al., 2009, A&A, 503, 379
Thielemann F.-K., Nomoto K., Hashimoto M.-A., 1996, ApJ, 460, 408
Thuan T. X., Balkowski C., Tran Thanh Van J., 1992, in Xuan Thuan T., Balkowski Ch., Tran Thanh Van J., eds, Physics of Nearby Galaxies: Nature or Nurture? Proc. 27th Rencontre de Moriond, Gif-sur-Yvette: Ed. Frontieres, p. 225
Timmes F. X., Woosley S. E., Weaver T. A., 1995, ApJS, 98, 617
Tinsley B. M., 1980, Fund. Cosm. Phys., 5, 287
Tornambé A., Matteucci F., 1986, MNRAS, 223, 69
Tosi M., 1996, in Leitherer C., Fritze-von-Alvensleben U., Huchra J., eds, ASP Conf. Ser. Vol. 98, From Stars to Galaxies: The Impact of Stellar Physics on Galaxy Evolution. Astron. Soc. Pac., San Francisco, p. 299
Trimble V., 1991, Astron. Astrophys. Rev., 3, 1
Tully R. B., Fisher J. R., 1977, A&A, 54, 661
Tully R. B., Mould J. R., Aaronson M., 1982, ApJ, 257, 527
Twarog B. A., 1980, ApJ, 242, 242
van den Bergh S., 1962, AJ, 67, 486
van der Kruit P. C., 1986, A&A, 157, 230
van Zee L., Haynes M. P., 2006, ApJ, 636, 214
Weidemann V., 2000, A&A, 363, 647
Whitford A. E., 1962, in Cunliffe McVittie G., ed., Proc. IAU Symp. 15, Problems of Extra-Galactic Research. Macmillan Press, New York, p. 27
Wirth A., 1981, AJ, 86, 981
Woosley S., Janka T., 2005, Nat Phys., 1, 147
Woosley S. E., Weaver T. A., 1995, ApJS, 101, 181
Wyse R. F. G., 2006, Memorie della Societa Astronomica Italiana, 77, 1036
Wyse R. F. G., Silk J., 1989, ApJ, 339, 700
Zaritsky D., Kennicutt R. C., Jr, Huchra J. P., 1994, ApJ, 420, 87

This paper has been typeset from a TEX/LATEX file prepared by the author.

Downloaded from https://academic.oup.com/mnras/article/415/2/1155/1034920 by INAF –IASF Bologna user on 17 January 2023